POLITECNICO DI TORINO

Master's Degree in Biomedical Engineering

Master's Degree Thesis

Inductive Power Transfer Class-E Amplifier Design for Active Implantable Medical Devices

Supervisors

Prof. Danilo DEMARCHI

Ph.D. Paolo MOTTO ROS

M.Sc. Fabiana DEL BONO

Candidate

Damiano MERLIN

December 2022

Abstract

Active Implantable Medical Devices (AIMDs) are continuously evolving; nowadays, though the devices are always much more complex and sophisticated, the power supply is a common challenge. It must guarantee safety, durability, and efficiency. A common technique is Wireless Power Transfer (WPT), and Class-E amplifiers are a possible solution in high-efficiency power amplifier (PA) applications. In the literature, higher frequencies begin to be more studied, principally to reduce coil dimensions and orientation sensitivity. The aim of this work is the development of a Wireless Power Transmitter through a Class-E amplifier at a carrier frequency of 13.56MHz (ISM radio band); the performance of the device developed has been evaluated to assess the capability of this solution in WPT.

The device has been initially simulated to size the components of the circuit correctly: LTspice and Python environments have been interfaced to optimize design choices, the solution with the highest efficiency is searched through an automatic algorithm. It consequently runs different LTspice simulations, varying through specific patterns the component values of the model, searching for an optimum efficiency that guarantees the minimum level of power delivered desired. Afterward, the prototype was tested on a breadboard; a simple receiver was developed for preliminary verification of the transmitter. A Printed Circuit Board (PCB) was then designed and fabricated; due to the radio frequency (RF) application, particular constraints were considered during the system's development. Power dissipation, efficiency, thermal performance, and the comparison with the expected transistor drain voltage and current behavior have been analyzed. A specific current sensing circuit has been designed and developed to support precise and accurate measurements.

Lastly, a testbench has been developed to better evaluate the performance test in different conditions. It guarantees an accurate variation of distance, misalignment, and angle between the transmitter and the receiver. Both distance and misalignment have been tested up to 20mm, while the angle has been tested up to 3 degrees.

In the future, integration into a complete WPT system is recommended to better study the device's performance and capability. The design of a power management system, that changes the transmitter output power based on the power delivered to the receiver, could give more robustness to the actual solution.

Table of Contents

List of Tables

List of Figures

Acronyms

AIMD
Active Implantable Medical Device

IMD
Implantable Medical Device

WPT
Wireless Power Transfer

Tx
Transmitter

Rx
Receiver

PA
Power Amplifier

RF
Radio Frequency

DC
Direct Current

SRF
Self Resonant Frequency

ASK
Amplitude shift keying

FSK
: Frequency shift keying

PSK
: Phase shift keying

r_{TX}
: Transmitted radius

r_{RX}
: Receiver radius

P_T
: Transmitted Power

PTE
: Power Transfer Efficiency

PDL
: Load Delivered Power

V_{IN}
: Input Voltage

PCB
: Printed Circuit Board

RMS
: Root Mean Square

BGA
: Ball Grid Array

BoM
: Bill of Materials

IC
: Integrated Circuit

GBW
: Gain Bandwidth Product

Chapter 1

Introduction

1.1 Active Implantable Medical Devices

According to FDA, an Implantable Medical Device (IMD) is a «device that is placed into a surgically or naturally formed cavity of the human body and is intended to remain there for a period of 30 days or more» [1].
IMDs can be divided into active and passive devices based on their requirement for a power source. Nowadays, IMDs technologies have been used to treat chronic diseases in different parts of the body, such as the brain, cochlea, retina, heart, lungs, and knee joints [Fig. 1.1]. Around three million people worldwide had pacemakers, and 600.000 more pacemakers were placed each year, according to statistics from two decades ago [2].
The active implantable medical devices (AIMDs) market is driven by several major factors, including the aging population and the related rise in the prevalence of chronic degenerative diseases, as well as improvements in healthcare quality and an expansion of the number of patients treated [3]. The firsts pacemaker implants procedure increased from 36823 to 49716, according to an analysis of temporal trends (2001–2017) of the National Hospital Discharge Database (HDD) about pacemaker (PM) and implantable cardioverter–defibrillator (ICD) procedures in Italy [4]. This increase was also brought on by the population's mean age, which rose from 76 to 78. Focusing on patients younger than 50, the number of 1st implants increase from 648 to 794 [4].
Power management is one of the most common problems in AIMDs; different solutions in the past years have been proposed: Lithium batteries, Bio-Fuels Cells, Nuclear Batteries, Thermoelectricity, Piezoelectricity, optical charging, and inductive coupling [2], that could be used with both rechargeable batteries and to directly power the device.

For deeper IMDs, the specifications are dictated by power requirements, longevity, and size of the power supply: medically, transcutaneous wire-based power sources are unacceptable because they significantly damage the tissue around the IMD; packaged batteries necessitate repeated surgical intervention to replace them due to their limited lifetime. Otherwise, batteries occupy an important portion of the device, and any leakage could be a severe risk to the patient's health. WPT is the potential solution that fulfills all of these requirements, enabling a more extended and safer operation of IMDs. Different WPT techniques have been studied and improved in the last two decades, such as Near-field resonant inductive coupling (NRIC), Near-field Capacitive Coupling, Ultrasound based wireless systems, Solar power harvesting, Electromagnetic Mid-Field based systems, and Electromagnetic Far-Field based systems [5].

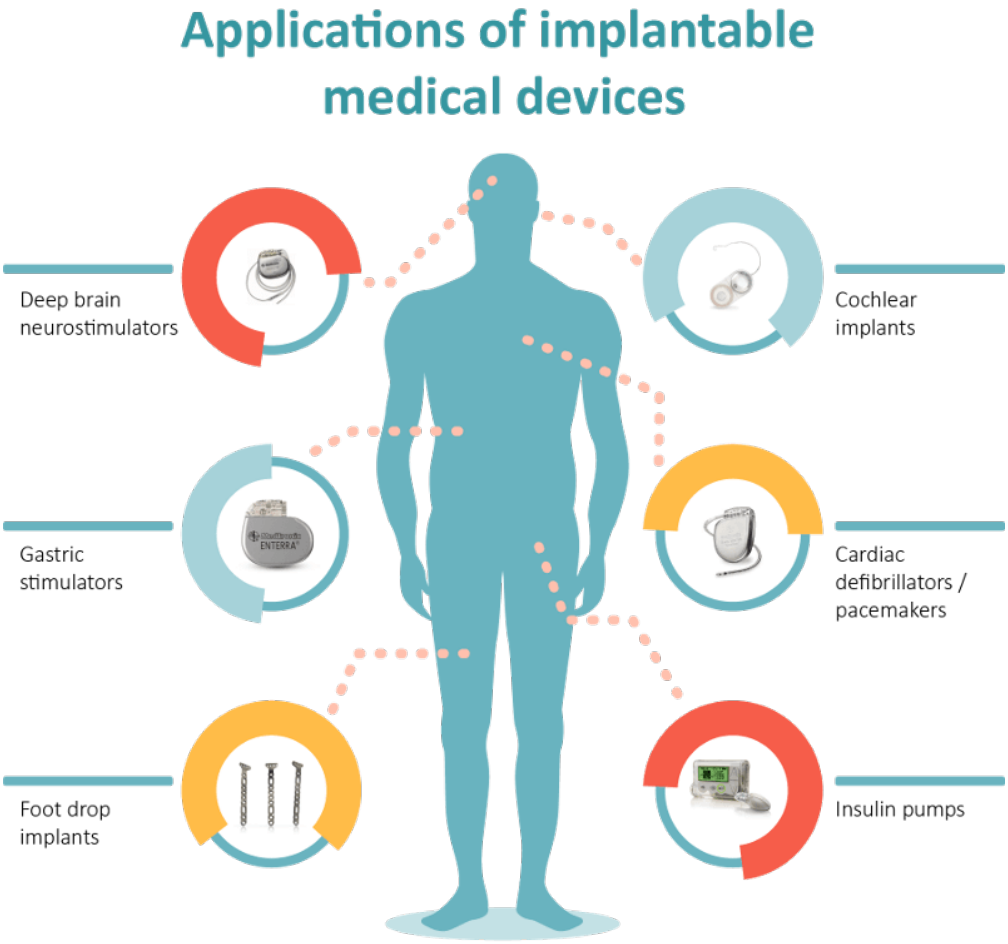

Figure 1.1: Active Implantable Medical Devices [6]

1.2 Inductive Power Transfer Class-E Amplifier design

The aim of this thesis is the development of a high-efficient IPT transmitter.
This project is correlated with two research projects: the SenseBack, an Implantable System for Bidirectional Neural Interfacing developed by the Imperial London College [7]; the remotely controlled implantable nanofluidic platform for tunable drug delivery developed by the Houston Methodist Hospital [8]. Both these active implantable medical devices are actually powered by a wireless power system working in the range of kHz.
This thesis aims to investigate the potential advantages obtained by shifting the power system to 13.56 MHz, with a study focused specifically on the transmitter; the constraints dictated by the device's power needs, temperature and size have been considered.
State of Art in IPT Class-E PA design was initially investigated; afterward, the transmitter was developed through the following steps:

- LTspice simulation
  - Firstly, the transistor and the coil were selected, and the circuit was sized based on the indication in the literature.
  - The circuit theoretically sized was then evaluated through LTspice simulation, and a python optimization algorithm has been developed to improve the circuit size automatically. Two configurations were obtained with two different transistors.
  - Circuit performance analysis has been conducted, evaluating efficiency, transmitted power, and received power with changes in distance, input voltage, and load.
- Breadboard preliminary test
  - The Class-E PA prototypes were developed on a welding breadboard to evaluate the system functioning: the voltage waveforms in the main points of interest have been measured.
  - A RF current sensing circuit has been developed and tested for the implementation on PCB.

- PCB design and test
  - PCBs of the transmitter and a simple receiver were developed. RF components have been used when necessary, and the guidelines of RF PCB design have been followed.
  - A testbench has been developed to accurately control distance, lateral misalignment, and angle between the transmitter and the receiver.
  - The prototypes developed were evaluated through the behavior of the waveforms in the main points of interest, total efficiency, and coil temperature.

Chapter 2

State of Art

Wireless power transfer is a wire-free power transfer technology; there have been numerous proposals for wireless energy transfer during the past few decades, a few of the different inductive approaches suggested to power implantable devices include near-field inductive coupling, near-field capacitive coupling, mid-field coupling, and far-field coupling [9].

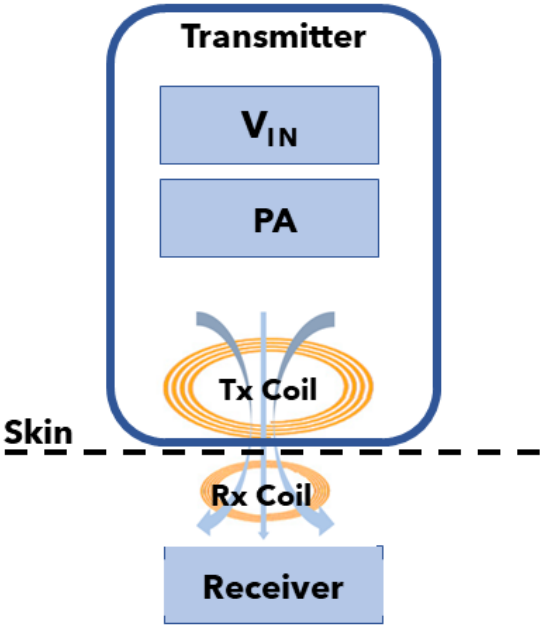

Figure 2.1: Inductive Power Transfer concept

WPT systems are normally categorized into two categories: near-field links and far-field links. This division is based on how they physically function; in the far field, energy is transported by electromagnetic waves, while in the near field, energy

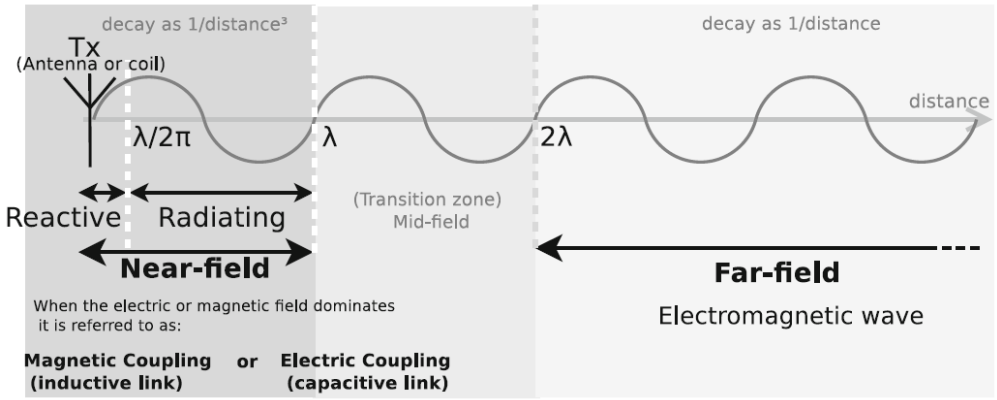

Figure 2.2: Near- and far-field approximated regions for antennas much shorter than the wavelength, λ. The WPT links are usually classified based on these operating regions [10].

is transferred via magnetic or electric coupling. Far-field is preferable for achieving great distances, in the range of meters, because the beam can be directed at the Rx. This beam-based WPT system can transmit via the air big power (kilowatts) over long distances (tens of meters) with an efficiency higher than 50%. According to the demand for biomedical applications, there is little requirement on the directivity and transfer range. However, the penetrability and power efficiency are extremely important [10]. Due to its higher efficiency and penetrability, near-field coupling appears to be more appropriate for biomedical applications [11]. Depending on the dominating field, the near-field can be further separated into the magnetic or electric coupling.

2.1 Inductive WPT

Inductive WPT is a logical choice for biomedical systems since the magnetic field negatively affects the human body less than the electric field. It can provide proper power levels and efficiencies [10]. The proximity of the two coils ensures a large use of the exciting magnetic flux and a high power transmission efficiency. WPT for medical devices typically operates in a recommended range between kHz and MHz due to the rise in electromagnetic energy absorption of the human body at higher frequencies [12].
A WPT link is highly influenced by parameters like the distance between Transmitter (Tx) and Receiver (Rx), their areas, and their relative orientation. In AIMDs, the Rx coil has the tightest size restrictions.

Other important parameters are the power carrier frequency, the Power Delivered to the Load (PDL), and the Power Transfer Efficiency (PTE); lastly, the total efficiency η_{TOT}, defined as the PDL over the power taken from the primary power supply (P_{IN}) [10].
A crucial condition of AIMDs design is the recharging time of the battery; it must not exceed a few hours and consequentially needs that the PDL satisfies the requirements.
A typical power transmission block diagram for AIMDs consists of two parts: the transmitter, external to the body, and the receiver implanted into the body [Fig. 2.3].

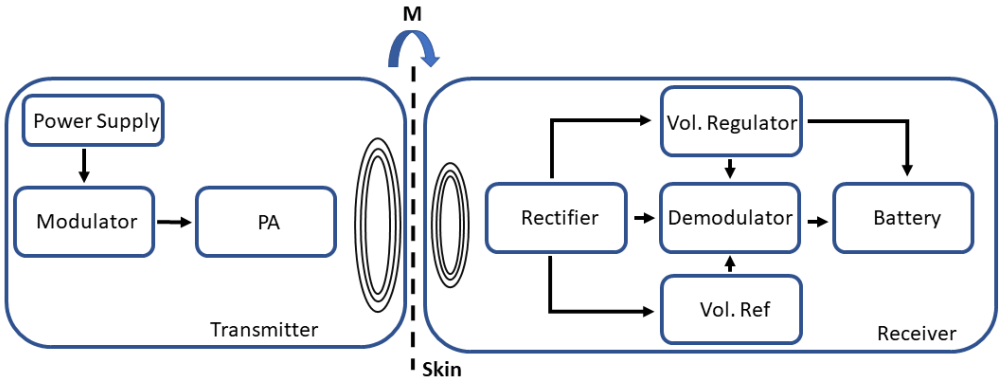

Figure 2.3: Schematic of a usual solution of a power transfer device for bio-implanted devices.

A Power supply, a Modulator, and a highly efficient PA are typical components of a transmitter. The modulator is optional, it is responsible for modulating the output of the transmitter based on receiver information; the power amplifier must ensure power transmission and efficiency objectives.
The receiver is made up of a demodulator, a voltage regulator, and a rectifier that extracts data and converts the RF signal to DC voltage, the power is transferred by use of a transmitter and a receiver coil connected by mutual inductance.
Different decisions have to be taken to correctly design the device:

- Carrier Frequency
- Resonant Topology
- Power Amplifier
- Coil design

2.2 Carrier frequency

The most common solution to efficaciously deliver wireless power to medical implants is low-frequency inductive coupling (< 10 MHz): at these frequencies, electromagnetic fields penetrate the body with minimal tissue heating [13].
Increasing the frequency of wireless power transmission into the body is still a work in progress since biological tissue has complex electrical properties. This intricacy comes from the numerous polarization processes present in tissues, and in particular, from the polarization frequency dependency.
At frequencies below 20 MHz, it is known that the power loss and specific absorption rate (SAR) via biological tissue are relatively minimal and can be neglected [14]. Recently, higher frequencies have been studied due to their lower orientation sensitivity and smaller and more efficient transmitter. At 1 GHz, a 10^4 times smaller antenna could be utilized to produce the same amount of power than it could at 10 MHz without increasing tissue absorption. Frequencies in the UHF band generally are suggested for a more efficient solution; however, often, the frequencies for maximizing the efficiency do not maximize the received power [13]. Depending on the application, the correct middle way has to be chosen.
The suitable frequencies are limited and regulated by international standards [Fig. 2.4]. Unlicensed frequencies are 130/150 kHz, 13.56 MHz, 868/915 MHz, 2.45 GHz, 5.2 GHz, and 5.8 GHz. In Europe, other frequencies can also be allowed in the range of 9-315 kHz [15].

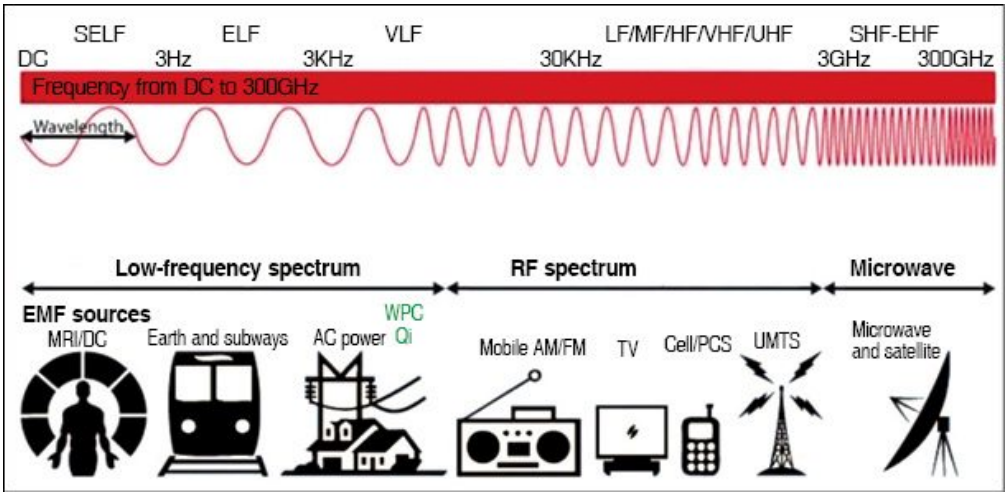

Figure 2.4: DC to 300 GHz frequency spectrum [16].

2.3 Resonant topology

Modeling the WPT system can be used different compensation configurations through C1 and C2 to reach magnetic resonant coupling and obtain higher efficiencies: [Fig. 2.5] [17]:

- SS: series-compensated primary coil; series-compensated secondary coil;
- SP: series-compensated primary coil; parallel-compensated secondary coil;
- PS: parallel-compensated primary coil; series-compensated secondary coil;
- PP: parallel-compensated primary coil; parallel-compensated secondary coil.

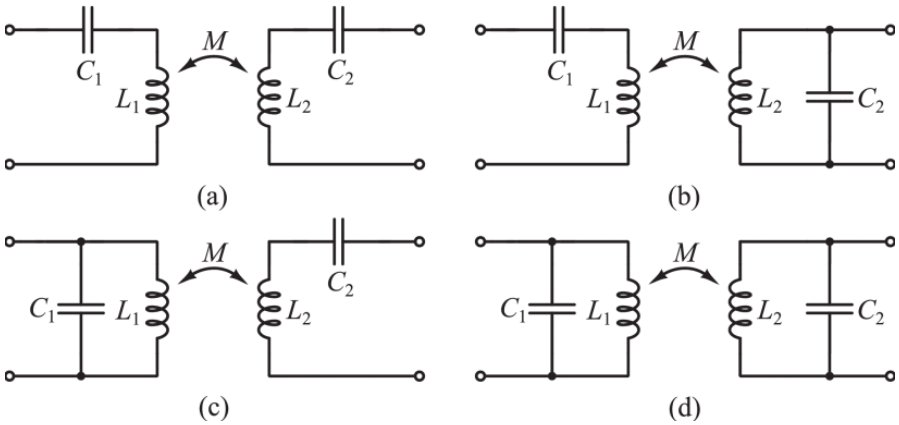

Figure 2.5: Comparison of NRIC link arrangements. (a) Series-Series (SS), (b) Series-Parallel (SP), (c) Parallel-Series (PS), (d) Parallel-Parallel (PP) [17].

In the literature, the issue of topology choice has been discussed, with various conclusions regarding when to adopt series and parallel-resonant topologies. The ideal output impedance for the SS arrangement is three orders of magnitude lower than the optimal output impedance for the SP link. Consequently, the SP link architecture is typical for biomedical inductive links; the driver is frequently a Class-D or -E amplifier suited to driving low impedances, in contrast to the receiver's normally moderately high input impedance [17]. From the observation of the results obtained by T. Campi, comparing different compensation configurations at 300 kHz and 13.56 MHz can be stated that higher efficiency has been reached from the SS configuration at 13.56 MHz [15].

2.4 Power amplifier

PAs are divided into classes. In Table 2.1 are presented different classes of PA and their relative efficiency.

Power Amplifier Types	**Approximate Efficiency (Theoretical)**
Class A	35 %
Class B	50 %
Class C	65 %
Class D	80 %
Class E	90-95 %
Class F	95 %

Table 2.1: Comparison of Class Power Amplifier Efficiency [18].

To power the transmitter coil, Class-E PA is widely used [18, 19, 20, 21, 22] in front of other Power Amplifier due to its high theoretical efficiency of 90 - 95 %, simple configuration (requires only one active device), high energy transmission, and low-power consumption when used as a modulator as it eliminates the need for a mixer [23]. On the other hand, this class of PAs has a narrow bandwidth [22].

2.4.1 Class E Power Amplifier

Class E Amplifier is firstly proposed by Nathan O. Sokal in 1975: «Advantages of Class E are unusually high efficiency, a priori designability, large reduction in second-breakdown stress, low sensitivity to active device characteristics, and potential for high-efficiency operation at higher frequencies than previously published Class-D circuits» [24].

The schematic of a Class E power Amplifier is presented in Figure 2.6.

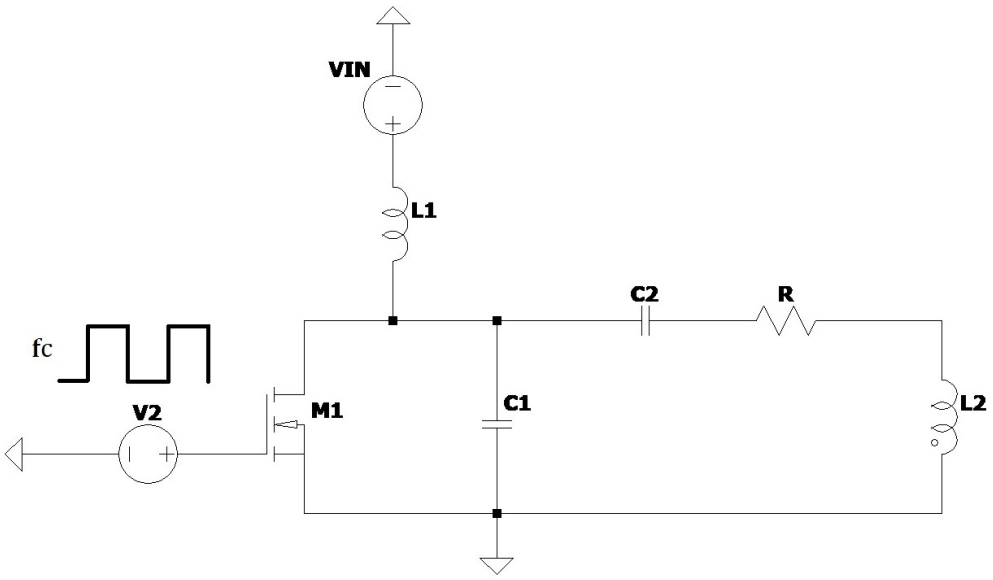

Figure 2.6: Typical Class-E Amplifier schematic

The transistor is the active output device; in the ideal condition, it functions as an ideal switch, with infinite off-resistance, zero switching times, and zero on-resistance [25]. The load network consists of [26]:

- a power choke inductor, it must be large enough to neglect its current ripple at the switching frequency
- a shunt capacitance C1
- a series tuned LC resonant circuit that acts as a filter for the harmonics
- a load R that is dependent on the application

The major losses in power amplifiers take place in the active output devices; the theoretical efficiency of class E PA is 100% if the following constraints are met [27] [Fig. 2.7]:

1. The rise of transistor voltage is delayed until after the current has reduced to zero;

2. The transistor voltage returns to zero before the current begins to rise.

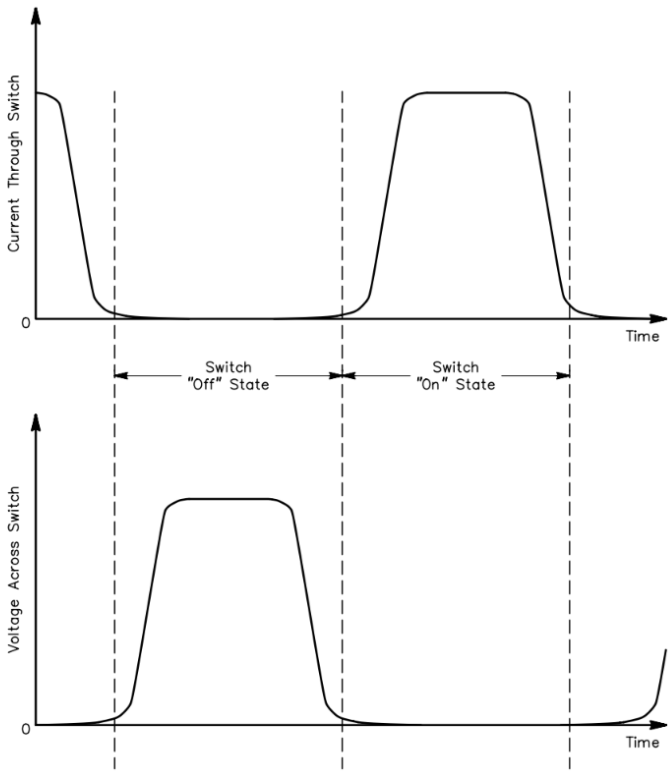

Figure 2.7: Conceptual "target" waveforms of transistor voltage and current [27]

Knowing that power is defined as $P = VI$, if V and I are commutate perfectly from zero to high level, the power dissipated is null.

Different equations have been proposed to design Class-E PA [19, 23, 27]; often, they are initially designed following the A. Grebennikov equations:

$$R = \frac{1.365 V_{IN}^2}{P} \tag{2.1}$$

$$L1 = \frac{0.732 R}{2\pi f_C} \tag{2.2}$$

$$C1 = \frac{0.685}{2\pi f_C R} \tag{2.3}$$

$$C2 = \frac{1}{2\pi f_C R Q} \tag{2.4}$$

$$L2 = \frac{1}{(2\pi f_C)^2 C2} \tag{2.5}$$

Afterward, the solution is usually tested and optimized through electronic simulation software like LTspice, Simulink [18], OrCAD-Pspice [23]. From the literature could be observed that it is often obtained efficiency higher than 80% [14, 19, 20, 21].

2.5 Coil design

Different key factors influence the coil design: smaller coil size and a greater data rate are achievable with a higher carrier frequency, yet tissue absorption rises with frequency [21]. Printed circuit board (PCB) spirals, «pancake» coils, and short wire solenoids are the most common coils employed [17]. The geometric parameters directly influence the electrical parameters: inductance, resistance, and capacitance. Geometric factors must be taken into account in the design of the coil, especially for the receiver coil implanted into the body.

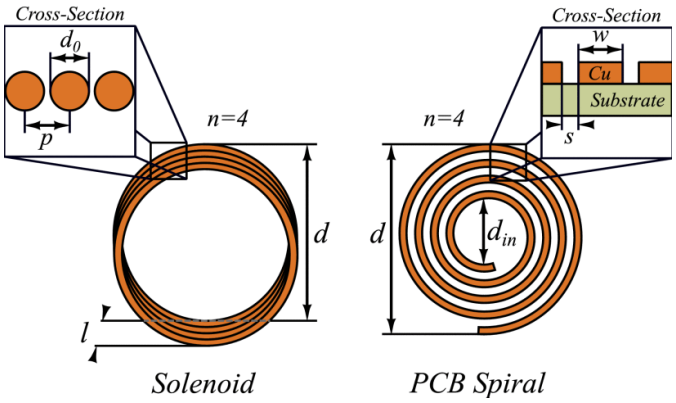

Figure 2.8: Solenoidal and spiral coil structure [17].

Moreover, the electrical parameters must satisfy the constraints imposed by the Class-E amplifier.
The main parameters of the coil are the inductance, the series resistance, normally reported on the datasheet, and the parallel capacitance. If the parallel capacitance is not annotated on the datasheet, it could be estimated by the self-resonant frequency (SRF).

$$f_{SRF} = \frac{1}{2\pi\sqrt{LC_P}} \tag{2.6}$$

Being the receiver coil implanted with the device into the body, the current must not produce excessive heating. Therefore, the receiver coil must be built with few turns and conductors with a wide cross-section to reduce resistive losses and, consequently, thermal dissipation.
A well-known method known as the geometric approach involves choosing a secondary coil diameter smaller than the principal, reducing the impact of coil misalignment on the voltage gain [21].

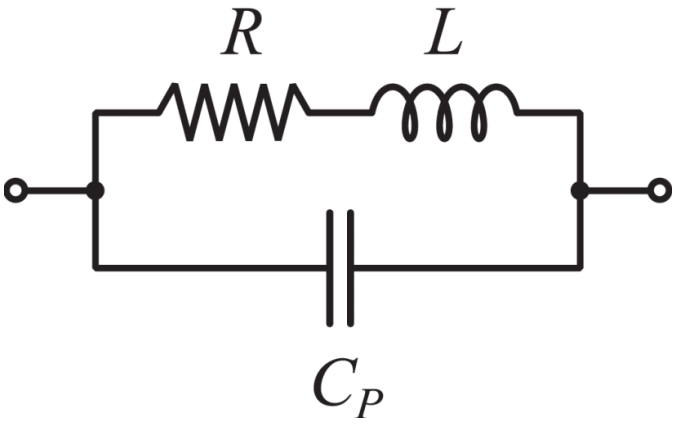

Figure 2.9: WPT coil electric model [17].

2.6 Modulator Design

The modulator is an electronic device used to modulate binary signals. Amplitude-shift-keying (ASK), frequency-shift-keying (FSK), and phase-shift-keying (PSK) are some of the modulation techniques utilized in implanted devices and bio-telemetry systems; each of these approaches has its benefits and drawbacks.
In the Class-E Power Amplifier design, the Q should be raised to improve the power transfer efficiency (PTE). But when the Q rises, the amplifier's bandwidth is reduced, and its sensitivity to changes in the frequency (or phase) of the input clock signal increases.
As a result, it has been difficult to execute FSK or PSK modulations on a Class-E PA, while ASK modulation is relatively simple to perform by modulating the supply voltage [22]. Other perspectives have been explored; a possibility is to modulate both the value of the shunt capacitor C1 and the RLC circuit; the architecture is presented in Figure 2.10.

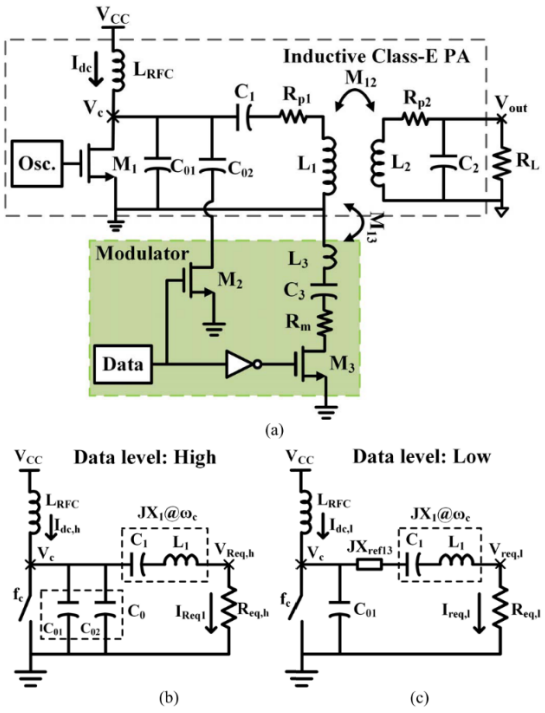

Figure 2.10: Description of the class-E modulator proposed by Navaii, (a) Block diagram of the proposed power and data transfer system (b, c) circuit model of the tuned class-E modulator for two data levels: high and low, respectively [21].

Chapter 3

Class-E PA design

3.1 Preliminary circuit layout

In designing the Class-E PA, the following items have been initially defined:

1. carrier frequency of 13.56 MHz, to reduce the misalignment sensitivity remaining in a safety range about the heat of tissues

2. usage of series to parallel topology based on the literature

3. selection of a WPT coil available on the market.

The circuit has been simulated on LTspice, a software produced by semiconductor manufacturer Analog Devices: «LTspice® is high-performance SPICE simulator software, including a graphical schematic capture interface. Schematics can be probed to produce simulation results—easily explored through LTspice's built-in waveform viewer» [28].
A Class-E PA is composed of two inductors, two capacitors, and one transistor. The transistor has to be accurately chosen to obtain high efficient setup.
Grebennikow equation considers an ideal situation; in the actual case, parasitic components influence the behavior of the circuits. Consequently, the use of an electronic simulator is recommended. In LTspice schematic, resistors, inductors and capacitors are added specifying their nominal value and, if needed, their parasitics. More complex components could be added through libraries, usually provided by the manufacturer.
The transistor influence on the output of the circuit could be very strong; the results of the simulation may not reflect the real output of the circuits, the manufacturers indeed specify that their Spice model cannot substitute breadboard testing, and cannot represent the exact device performance under all conditions. LTspice results will be useful in understanding the circuit behavior but will not be taken for

granted.
As discussed before [Fig. 2.3] the transmitter could be divided into three main parts; the ASK modulator would not be considered in this study.
Different methods and equations have been proposed for the initial sizing of the circuit; whichever equations are being used, some rules must be respected:

- The RLC circuits have to be at resonance at the carrier frequency;
- The power choke inductor needs an inductance value bigger than the transmitter coil to reduce its ripple current.

3.1.1 WPT Coil

In a Class-E PA, being the transmitter Coil part of the RLC circuits, to correctly operate the device, it must be respected the condition of resonance, given by the correct combination of values of the capacitor and the inductor. Consequentially, if the inductance value is unstable, the resonance condition could easily fail. A non-resonant design will have lower efficiency [17].
Productors such as Wurth, TDK and Vishay do not currently have catalog availability of coils produced to be used at 13.56 MHz, most of the coils sold are produced to be used at 100 kHz. These coils, if used at higher frequencies, have a high inductance variability.
Two coils sold respectively by TDK and Wurth electronics were considered: WT151512-22F2-ID and 760308101106, both these Qi standard coils are produced to be used at 100 kHz. The two coils have been characterized in the range between 10 kHz and 16 MHz through the 4294A Agilent impedance analyzer, in order to understand whether they were usable [Fig. 3.1].
The impedance analyzer outputs are respectfully frequency, phase, and magnitude of impedance. With these data, the inductance, resistance and impedance could be found through the following equations:

$$R = Re(Z) = Z\cos\phi \tag{3.1}$$

$$Z = Im(Z) = Z\sin\phi \tag{3.2}$$

$$L = \frac{Im(Z)}{2\pi\phi} \tag{3.3}$$

The analysis of both the coils shows how the range of linearity end at 1 MHz; above 5 MHz, the non-linearity effects are predominantly influencing the value of the inductance and the resistance.

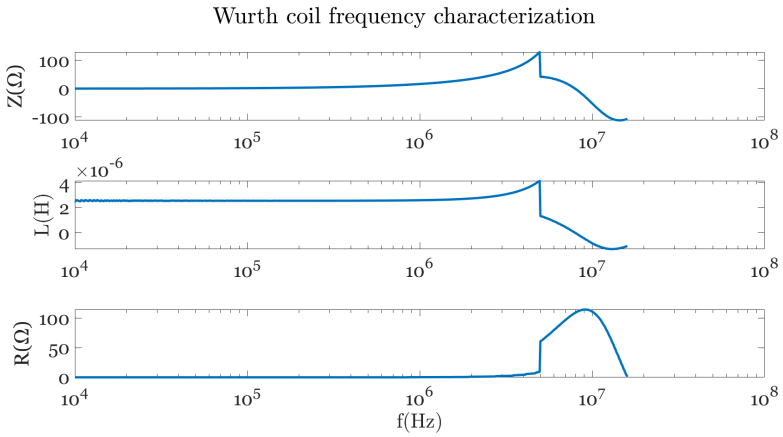

(a) WT151512-22F2-ID

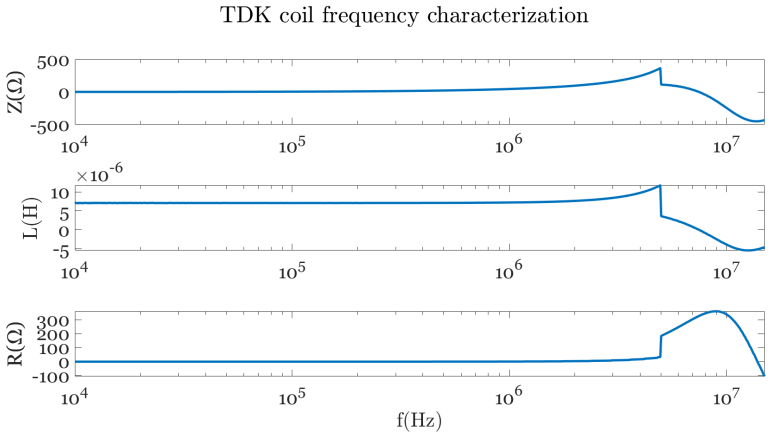

(b) 760308101106

Figure 3.1: Characterization of WPT coils through an impedance analyzer

There is low availability of coils produced for higher frequency on the market. Moreover, the higher the frequency, the smaller the dimension of the coil. Grupopremo produces the ZC1003HF [Fig. 3.2], coils especially realized for 13.56 MHz applications. Two models are available, respectively, with inductance and series resistance values of 2.2 µH - 130 mΩ and 4.5 µH - 380 mΩ. Both will be considered, trying to understand if one value permits reaching better circuit performance.

The size of the coils is pretty small [Fig. 3.2]: from the datasheet, the case is 10 mm in diameter, while the external diameter of the coil is 6 mm; in an optimal situation, a larger coil permits to have fewer misalignment errors, but based on the market availability this is the best solution found.

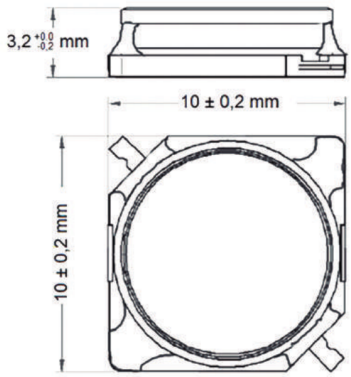

Figure 3.2: ZC1003HF dimensions

3.1.2 Resonant Capacitor

The resonant frequency of an LC circuit is related to the following equation:

$$f = \frac{1}{2\pi\sqrt{LC}} \tag{3.4}$$

Knowing the desired frequency (13.56 MHz) and the inductance value of the coil (2.2 µH and 4.5 µH), the value of the series capacitor could be obtained:

$$C = \frac{1}{(2\pi f)^2 L} \tag{3.5}$$

As a result, capacitance of 30 pF and 62 pF have been sized, respectively, for the coil of 4.5 µH and 2.2 µH inductance.

3.1.3 Power Choke Inductor

The choke inductor must be large enough to neglect its current ripple at the switching frequency [25]; to do that, a typical choice is to take an inductance of one magnitude greater than the transmitter coil inductance:

$$L1 = 10 \cdot L2 \tag{3.6}$$

As a result, choke inductor values of 22 µH and 45 µH have been chosen, respectively, for the two models of the ZC1003HF coils.

3.1.4 Power Transistor

To select the most proper transistor its parasitics must be accurately studied from the datasheet; its main characteristics, which influence the behavior of the circuit, are the following:

- C_{ds}, a capacitance parallel to the transistor, that in the Class-E PA contributes to the value of C1
- $R_{DS(ON)}$, a series resistance on the drain, increases the power dissipated on the transistor when the condition of ideal switch voltage is not strictly respected.
- $t_{ON/OFF}$, the transistor timing has to be fast enough to create a square wave at the frequency chosen.

Usually, the datasheet reports the input, output, and reverse capacitance; from these values could be calculated the parasitic capacitance of Figure 3.3 through the following relations:

$$InputCapacitance(C_{iss}) = C_{gd} + C_{gs} \tag{3.7}$$

$$OutputCapacitance(C_{oss}) = C_{ds} + C_{gd} \tag{3.8}$$

$$ReverseTransferCapacitance(C_{rss}) = C_{gd} \tag{3.9}$$

Combining C_{oss} and C_{iss} could be found C_{ds}:

$$C_{ds} = C_{oss} - C_{rss} \tag{3.10}$$

To understand the ideal values of the transistor timing, if it is used a 50% duty cycle (DC) wave, t_{ON} and t_{OFF} must be smaller than half of the period T [Fig.

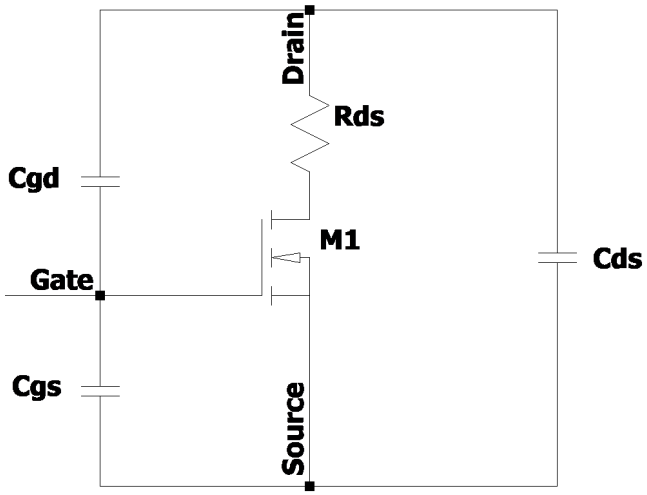

Figure 3.3: Model of transistor parasitics

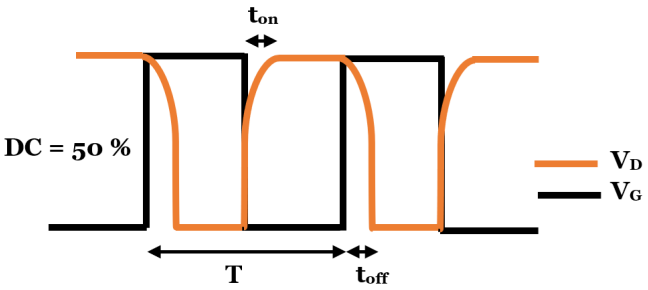

Figure 3.4: Transistor timing scheme of functioning

3.4], ideally one order of magnitude lower.

$$t_{ON/OFF} = \frac{T}{20} \tag{3.11}$$

Considering a frequency of 13.56 MHz, the period is equal to 73 ns; applying eq.3.11 could be observed how to operate in a safe range, the transistor timings needed are less than 3.6 ns.
A less stringent alternative can be found relating the timing to the turn-off dissipation desired. For example, to obtain a 6 % turn-off dissipation of the output power, and if Q, defined with the ratio of the inductor reactance and the resistor, is equal to 3, the allowable value for the timing can be found with the following

equation [27]:

$$\frac{t_{ON/OFF}}{T} = \frac{\sqrt{12(\frac{P_{d,t_{OFF}}}{P})}}{2\pi(1+\frac{0.82}{Q_L})} \tag{3.12}$$

From the literature, a typical transistor choice is the MOSFET 2N7000 [14, 20]. It has a maximum drain-source on-state resistance ($R_{DS(ON)}$) of 5 Ω, C_{ds} equal to 10 pF, and $t_{ON/OFF}$ respectively of 3 to 10 ns. GaN transistors have the advantage that, if compared with the relative MOSFET, have a $R_{DS(ON)}$ an order of magnitude smaller.
Different possibilities of the manufacturer GaN System have been explored: the Gs-065-004-1L, Gs-065-008-1L, and GS66508B. From Table 3.1 could be noted how effectively the GaN Transistor has lower $R_{DS(ON)}$ than MOSFET. The fastest transistor is the GS66508B, but it also has higher C_{ds}, parasitic capacitance in parallel to the shunt capacitor of the Class-E PA. During the simulation, the influence of these characteristics has been observed, and the transistor have been compared.

Transistor	$R_{DS(ON)}$ (Ω)	t_{ON} **(ns)**	t_{OFF} **(ns)**	$Ciss$ **(pF)**	C_{oss} **(pF)**	C_{rss} **(pF)**	C_{ds} **(pF)**	$V_{GS(TH)}$ **(V)**
2N7000	2.8	3	12	25	18	7.5	10.5	3.5V
Gs0650041L	0.450	3	11.5	26	7	0.3	6.7	2.6V
Gs0650081L	0.225	4.8	8	54	14	0.3	13.7	2.6V
Gs66508B	0.050	3.7	5.2	242	65	1.5	63.5	2.6V

Table 3.1: Comparison of the main characteristics of four transistors

3.1.5 Receiver model

The receiver has been schematized by a simple RLC circuit; the schematic is presented in Figure 3.5a. The transmitter and receiver coil are coupled by a mutual inductance M [17]; the coupling could also be described by the coupling coefficient K ($0 < K < 1$). The coupling coefficient could be obtained given the radius of the transmitter and receiver coils (r_{Tx},r_{Rx}) and the distance between them (d) [10]:

$$K = \frac{r_{Tx}^2 r_{Rx}^2}{\sqrt{r_{Tx} r_{Rx}}\sqrt[3]{d^2 + r_{Rx}^2}} \tag{3.13}$$

From the autoinduction coefficient K, it is always possible to obtain the mutual inductance M [10]:

$$M = K\sqrt{L_{Tx} L_{Rx}} \tag{3.14}$$

Another possibility to further simplify the schematic could be to include the receiver behavior through the reflected resistance R_{RXTX} generated by the coupling link in

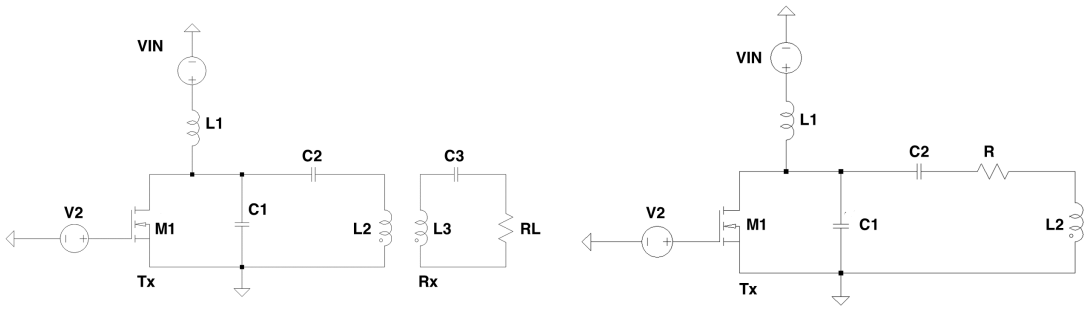

(a) Schematic with the representation of a simple RLC receiver

(b) Schematic with the receiver included in Zrxtx

Figure 3.5: Comparison of two possible representations of a WPT Class E-PA

the transmitter [Fig.3.5b]. To do that, we have to know the receiver load resistance (RL), the series resistance of the receiver coil, the inductance of the receiver and the transmitter coil, and the coupling coefficient [Eq. 3.15].

$$R_{RXTX} = \frac{2\pi f^2 K^2 L_{Tx} L_{Rx}}{R_{Rx} + RL} \tag{3.15}$$

All circuit elements, if considered ideals, do not dissipate real or active power other than resistors R [Fig. 3.5b]. Anyway, in actual solution, all the components have parasitics that must be taken into account, introducing dissipation.
To correctly develop a Class-E PA, almost all of the drawn power has to be delivered from V_{IN} to the apparent resistor R_{RXTX}, being the desired output power of the link. All the power dissipated due to parasitics is waste power, so the components must maintain their parasitics as low as possible [22].
The two possible schematics of Figure 3.5 will be compared to understand if different modeling of the same circuits could involve different results due to simulation issues. Initially, it is desired to observe the circuit behavior. R_{RXTx} is put equal to $50\,\Omega$, a typical value from the literature, and then its behavior has been evaluated referring to the load and the distance between the receiver and the transmitter.

3.1.6 Shunt Capacitor

From the previous consideration it could be easily observed how simply imposing the value of the coil leads to the choice of the choke and the capacitor. The Grebennikov equation could be used to calculate the value of the shunt capacitor C1 [Eq. 2.3]; a capacitor value of 160 pF has been designed. The initial sizing of the Class-E Amplifier is completed [Tab. 3.2] [Tab. 3.3].

Component	**Value**	**Rp**	**Cp**
L1	45 µH	-	-
L2	4.5 µH	380 mΩ	9 pF
C1	160 pF	-	-
C2	30 pF	-	-

Table 3.2: Class-E PA components sized with Grebennikow equations (coil of 4.5μH)

Component	**Value**	**Rp**	**Cp**
L1	22 µH	-	-
L2	2.2 µH	180mΩ	18 pF
C1	160 pF	-	-
C2	62 pF	-	-

Table 3.3: Class-E PA components sized with Grebennikow equations (coil of 2.2μH)

3.2 LTSpice simulation for an efficacious Class-E PA design

In LTspice simulations, once the circuit's components have been sized, a transitory of time must be set through the function «.TRAN». This function defines the time period in which the simulation lasts and must be longer than the initial transient needed to reach the stable condition. A transitory of 20 µs was initially chosen. LTspice samples the data non-linearly, with a variable step size. It is important to set up the parameter «maximum step size»; it defines the maximum step period admissible, increasing accuracy with a relative increase in the simulation time. Based upon the circuit carrier frequency, 13.56 MHz, a maximum step size of at least two orders of magnitude lower, equal to 0.1 µs, has been adopted.

3.2.1 Power Choke Inductor effectiveness

Figure 3.6 shows the results obtained by reducing the value of the choke inductor below the previously set threshold. It could be observed how the order of magnitude difference between L1 and L2 reduces the RF current component across the power choke inductor (L1).

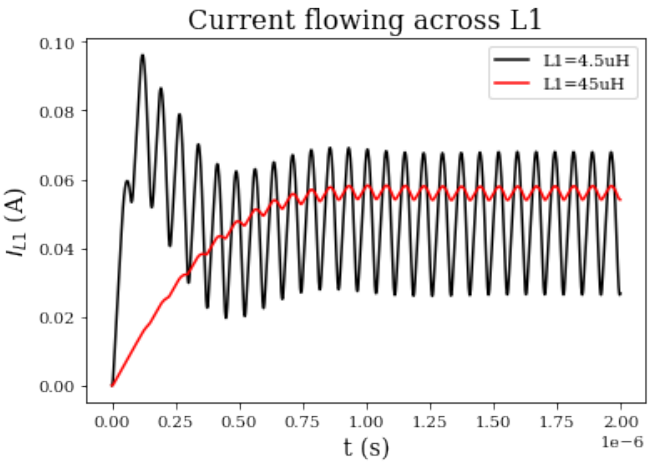

Figure 3.6: Influence of the inductance value on the current flowing across the power choke inductor

3.2.2 Transistor switch operation

The results in Figure 3.7 were obtained by simulating the previously sized circuit and showing the transistor voltage and current waveforms.

The waveforms obtained are far from the ideal condition. Current and voltage

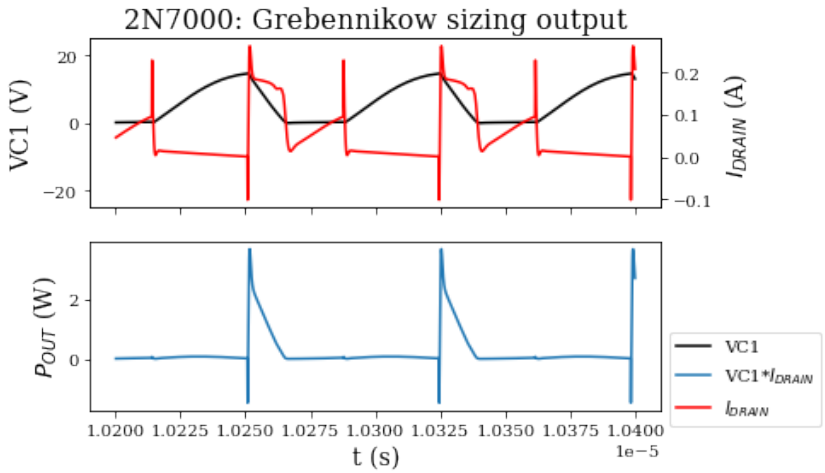

Figure 3.7: Waveforms of transistor voltage and current in the Class-E PA sized with Grebennikow's equation

behavior do not meet the requirements: their voltage and current waveforms are superimposed, so their product, which represents the power dissipated, is much higher than zero.

The ideal condition, with a theoretic efficiency of 100%, dissipates no power. The waveform in Figure 3.7 has been evaluated as dissipating an average power of 234 mW.

In the literature, Sokal has proposed a set of items to optimize the selection of the components' value based on the waveform conditions [27]. Figure 3.8 shows how to proceed with the evaluation: due to the delayed growth of Voltage on C1 [Fig. 3.7], the value of C1 must be decreased.

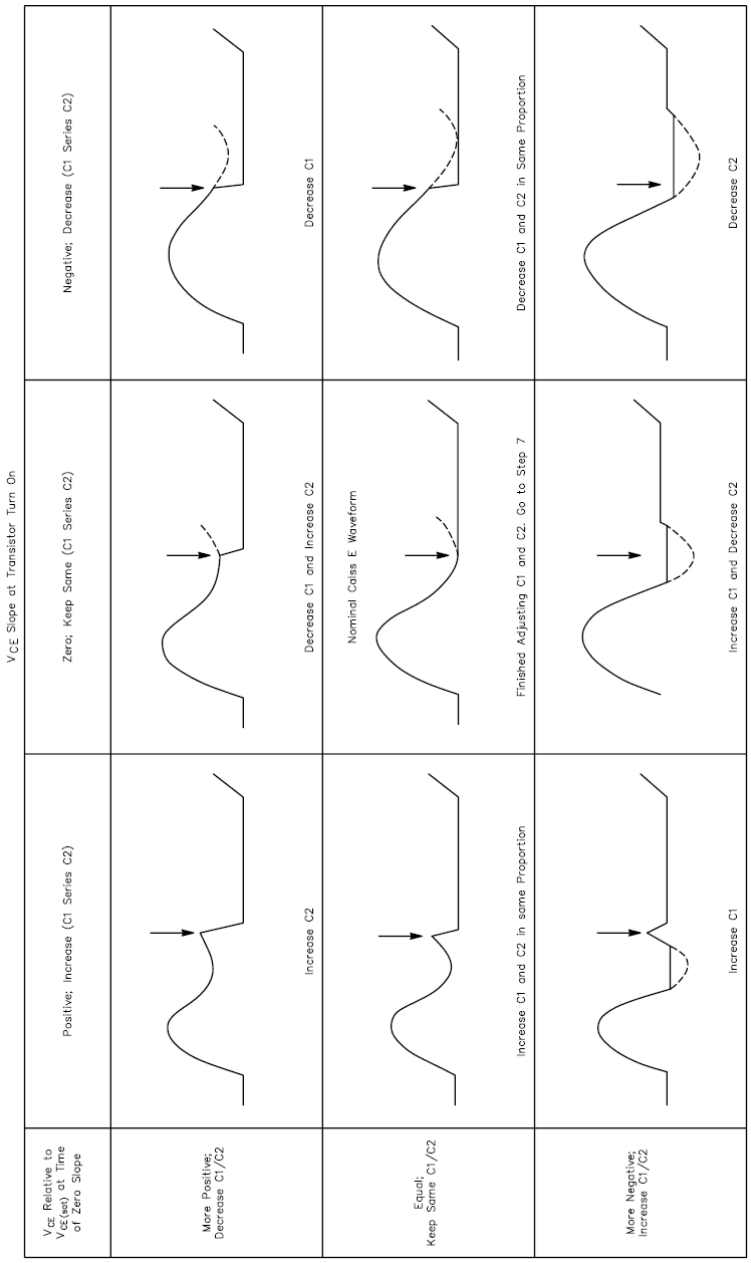

Figure 3.8: C1 and C2 adjustment procedure. The vertical arrow indicates transistor turn-on [27].

3.2.3 Transmitted Power

The transmitted output power (P_T) of the Class-E PA is obtained through the product of the transmitter coil voltage and current; its behavior has been investigated changing V_{IN} values of 5, 7, 10 and 12 V [Fig. 3.9].

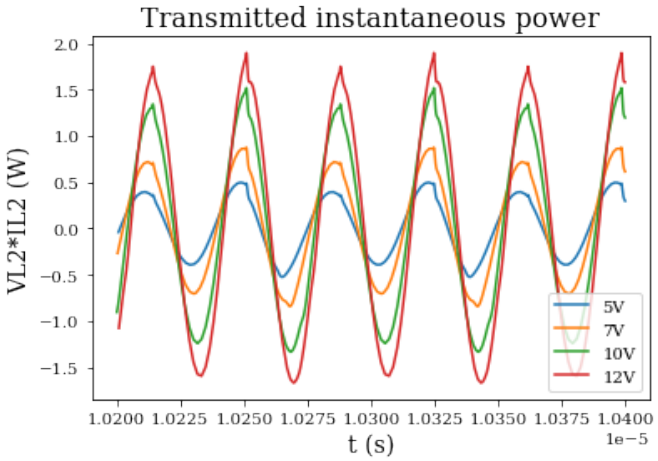

Figure 3.9: Instantaneous transmitted Power behaviour varying V_{IN}

Finding the optimum configuration through multiple trial and error attempts could be long and difficult. To automatize this procedure, making the optimal solution more accessible and faster to find, an algorithm for automatic optimum search has been developed in Python.

3.2.4 Python Optimization Algorithm

Python library PyLTspice allows running and modifying LTspice scripts. Usually, on LTspice, it is only possible to change component values through steps value; the use of Python for LTspice simulation allows for automated choices and decision-making during the data elaboration process. A simple optimization algorithm has been developed to achieve two main goals: minimum output power and proximity to the ideal Class-E amplifier transistor drain and current waveforms [Fig. 2.7], which could be resumed in a high PA efficiency.
The algorithm discards the solutions that do not fit with the first condition and search for the best solution based on the second, evaluating the efficiency. Based on the Sokal evaluation [Fig. 3.8], searching patterns have been defined; the values of the components have been altered in accordance with the following items and the efficiency has been calculated for each combination:

1. $L2 = 4.5\mu H - C2 = 30\,\text{pF}$ / $L2 = 2.2\mu H - C2 = 62\,\text{pF}$
2. $8L2 < L1 < 100L2$
3. $1\,\text{pF} < C1 < 10\frac{0.685}{2\pi f_C R}$
4. stop condition, based on a stop in the increase of efficiency

The optimization algorithm must be applied separately for each transistor. Initial testing was done with the MOSFET 2N7000; Figure 3.10 illustrates the results, which show a very low superimposition of voltage and current traces resulting in a decrease in power dissipation to 5 mW.

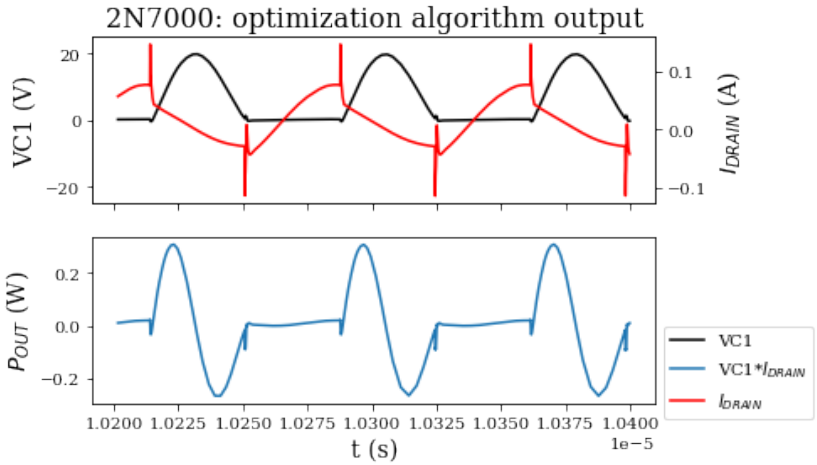

Figure 3.10: Waveform of transistor voltage and current in the 2N7000 Class-E PA sized with the optimization algorithm output

3.2.5 Transistor parasitics influence

The optimization algorithm has been initially tested with the MOSFET transistor 2N7000. The parasitic parameters and, consequently, the output of the PA vary when the transistors are changed. Figure 3.11 shows how, with the same-sized circuit (in this case, the circuit sized for the 2N7000), the voltage and current traces change significantly. The parasitic capacitance C_{ds}, sum up to the shunt capacitor C1; according to Sokal, as its value increases, the waveform changes as reported in Figure 3.8.
As a result, transistors with high C_{ds} are discarded because the value of C1 obtained from the optimization algorithm is small. Due to its high C_{ds} value, even if the GS66508B has the best timing, it must be discarded.

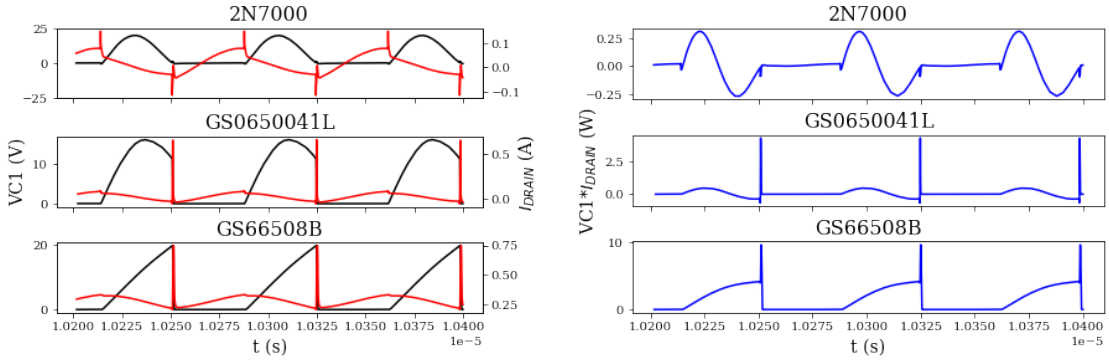

(a) Waveform of transistor voltage and current **(b)** Waveform of power across the transistor

Figure 3.11: Comparison of PA performance in the 2N7000-Class-E PA sized with the optimization algorithm output, varying the transistor

Better results were obtained by testing the optimization algorithm on the GaN transistor series and by uniting the 2.2 µH coil and the GS0650041L [Fig. 3.12], with an average dissipated power equal to 3 mW.

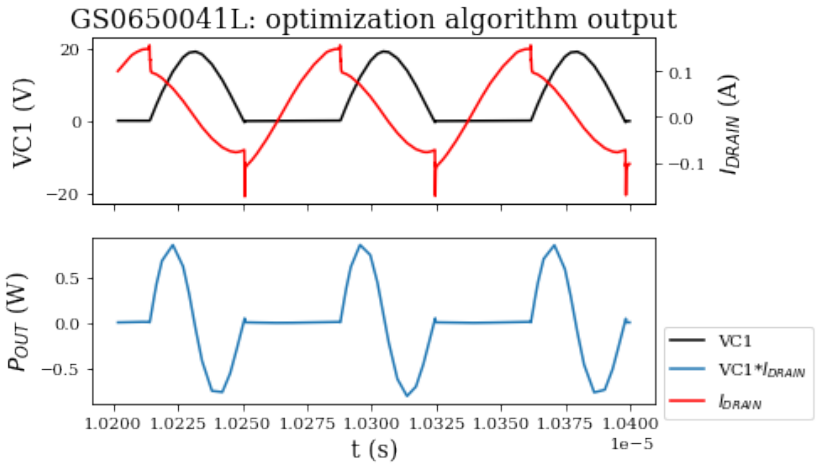

Figure 3.12: Waveform of transistor voltage and current in the GS0650041L Class-E PA sized with the optimization algorithm output

From now on, the two configurations obtained with the 2N7000 and the GS0650041L, respectively, known as «2N7000 Class-E PA» and «GS0650041L Class-E PA», will be analyzed. Consequentially, this study compares the performances of Class-E PA by using two different transistor technologies, GaN and MOSFET. Table 3.4 shows the final configuration of the two transistors.

Configuration	**L1**			**L2**			**C1**		**C2**	
	L(μH)	Rp(Ω)	Cp(pF)	L(μH)	Rp(Ω)	Cp(pF)	C(pF)	Rp(pΩ)	C(pF)	Rp(pΩ)
2N7000	40	0.18	0.11	4.5	0.38	9	13	20	30	20
GS0650041L	220	2.6	0.078	2.2	0.18	18	15	20	62	20

Table 3.4: Class-E PA components sized with the Python Optimization algorithm for the two configurations

3.3 Efficiency

3.3.1 Background

Efficiency could be calculated through powers ratio. According to the equation P=VI, where I is the current flowing through the element and V is the voltage across it, a circuit element either dissipates or creates power. In an AC circuit, both the current and the voltage are time-dependent. Hence the instantaneous power is likewise time-dependent.

$$P(t) = V(t)I(t) \tag{3.16}$$

I(t) and V(t) for a resistor are in phase and always have the same sign. Due to their phase differences, a capacitor's or an inductor's relative signs of I(t) and V(t) change during a cycle. As a result, P(t) is sometimes positive and negative, showing that capacitive and inductive components generate and absorb power at specific times [Fig. 3.13] [29].

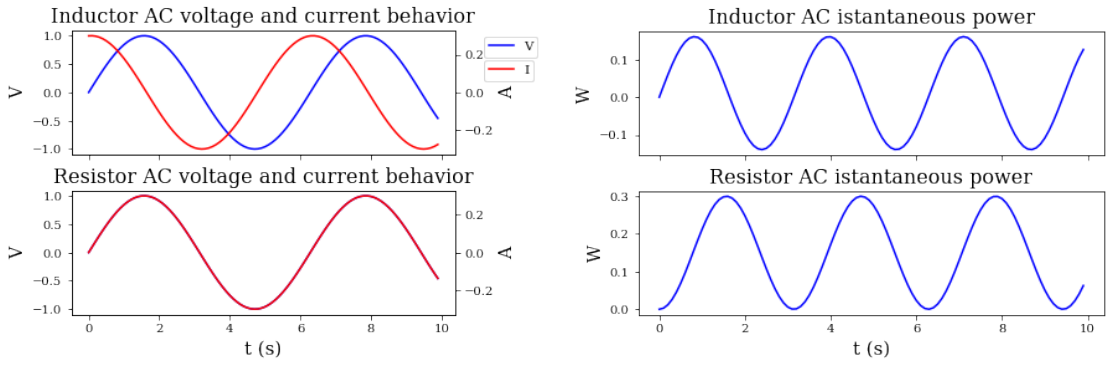

(a) Voltage and current behavior across a resistor and inductor

(b) Istantaneous power across a resistor and inductor

Figure 3.13: Expected voltage, current and istantaneous power behavior across an inductor and a resistor

Instantaneous power rarely has practical significance because it fluctuates over a cycle in magnitude and sign. The power averaged through time, often known as the average power, is what we are always interested in. It is determined by the instantaneous power's time average across a cycle:

$$P_{AVG} = \frac{1}{T}\int_0^T p(t)\,dt \tag{3.17}$$

The average power of an AC generator, in terms of RMS values, is written as follows:

$$P_{AVG} = V_{RMS} I_{RMS} \cos\phi \tag{3.18}$$

The difference between the power delivered in the circuit and its theoretical maximum, due to voltage and current being out of phase, is known as the power factor ($\cos\phi$) in engineering applications. Since $\phi = 0$ for resistors, the average power dissipated is as follows:

$$P_{AVG} = V_{RMS} I_{RMS} \tag{3.19}$$

The phase angle of an AC generator can be any value. When $\cos\phi > 0$, the generator generates energy; when $\cos\phi = 0$, it absorbs energy.
RMS values become more complicated to be calculated when the signal in the analysis is not sinusoidal; consequently, in our case, the average power have been calculated through integration, in particular through the numeric integration method trapz, available both on Ltspice and Python.

3.3.2 Class-E PA efficiencies of interest

Efficiencies of our interest could be divided into three different contributes:

1. Power Amplifier efficiency (η_{PA})
2. Link efficiency (η_{LINK})
3. Total efficiency (η_{TOT})

The total efficiency is also equivalent to the product of the previous. To calculate all the efficiencies, the ratio between the average powers is needed.
The results obtained from the simulation must be carefully observed. LTspice simulates the expected behavior of the circuit, but with complex simulations its accuracy could decrease.
In WPT Class-E Amplifier, the complexity of the simulation increase due to three factors; the transistor model is usually given by the manufacturer, which explains how its model is not intended to substitute proper testing on a breadboard. In particular cases, the simulation output could not represent the actual case. The carrier frequency belongs to the RF range, increasing the complexity of the simulation. The influence of the parasitic components becomes important and can change the waveform behavior.
The model of the inductive link is difficult to represent and adds complexity.

To study the efficiencies of interest, the average power must be calculated in four nodes of the circuit [Fig. 3.14]:

1. Input Power (P_{IN})
2. Transmitted Power (P_T)
3. Received Power (P_R)
4. Load delivered Power (PDL)

Once the values of these powers have been calculated, the efficiencies can be obtained using the following equations:

$$\eta_{PA} = \frac{P_T}{P_{IN}} \tag{3.20}$$

$$\eta_{LINK} = \frac{P_R}{P_T} \tag{3.21}$$

$$\eta_{TOT} = \frac{PDL}{P_{IN}} \tag{3.22}$$

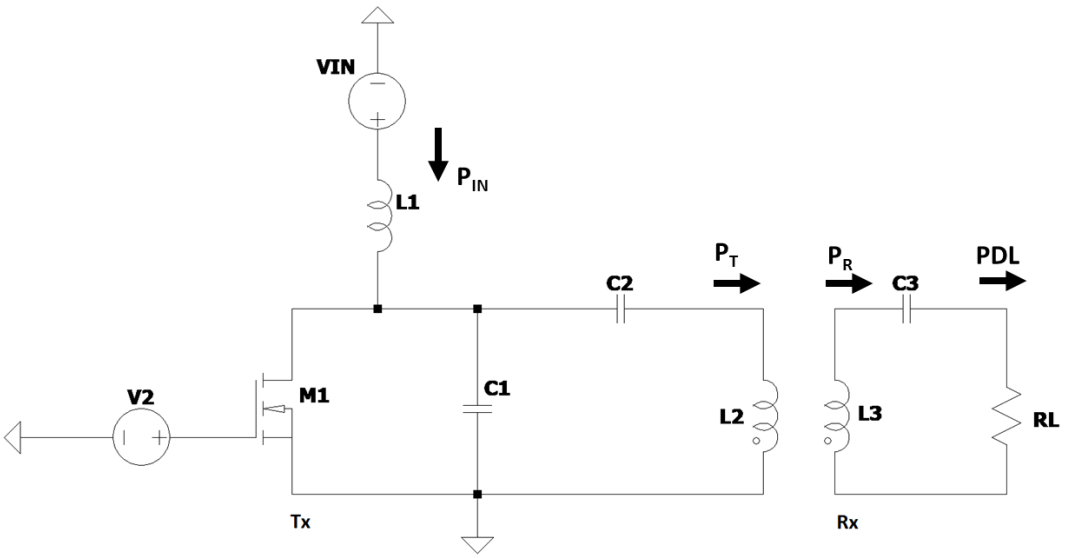

Figure 3.14: Efficiencies and power of interest in the Class-E Amplifier

The data of simulations have been imported and elaborated in Python. Calculated the instantaneous power, the average power has been found through integration, with the trapz function relative to the scipy library. This function applies the composite trapezoidal rule to the signal. It is necessary to take into consideration the time vector input parameter, which is crucial due to LTspice's non-linearly sampled data.
To better exploit the circuit behavior, from now on, the simulations have been conducted on the circuit of Figure 3.14, with transmitter and receiver contributions separated, guaranteeing a deep study of the receiver.

3.3.3 Transmitted power and efficiency distance variability

Starting from the instantaneous power, it can be observed how the behavior of the waveform across L2 and RL follows the expectations [Fig. 3.15].
Then, 10 K values relative to 10 distances, from 0 mm to 20 mm with a step of

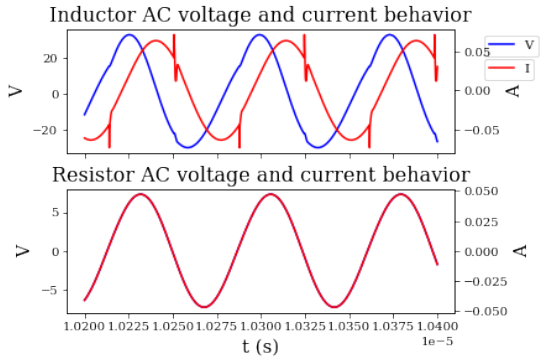

(a) Voltage and current behaviour respectively on L2 and RL

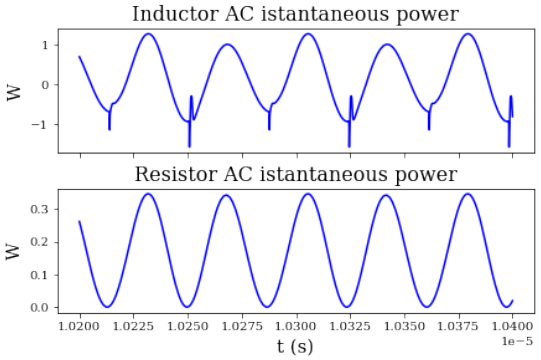

(b) Istantaneous power respectively on L2 and RL

Figure 3.15: Waveforms of voltage, current and istantaneous power on L2 and RL of the Class-E PA

2 mm, have been calculated through the equation 3.13, by exploiting the circuit's output dependence on the distance.
For each step, efficiencies, P_T, and PDL have been evaluated, both for the 2N7000 and the GS0650041L configurations, obtaining the following results.
From the power transmission behavior, the transmitted power was very similar to the power delivered to the load [Fig. 3.16]; this is coherent with the high link efficiency observed [Fig. 3.17]. In fact, η_{TOT} is obtained by multiplying η_{PA} with η_{LINK}. Moreover, comparing η_{TOT} with the simulation results of the equivalent circuit represented with the R_{RXTX} schematic [Fig. 3.5b], the results are similar; the difference of efficiencies obtained never exceeds 7%.

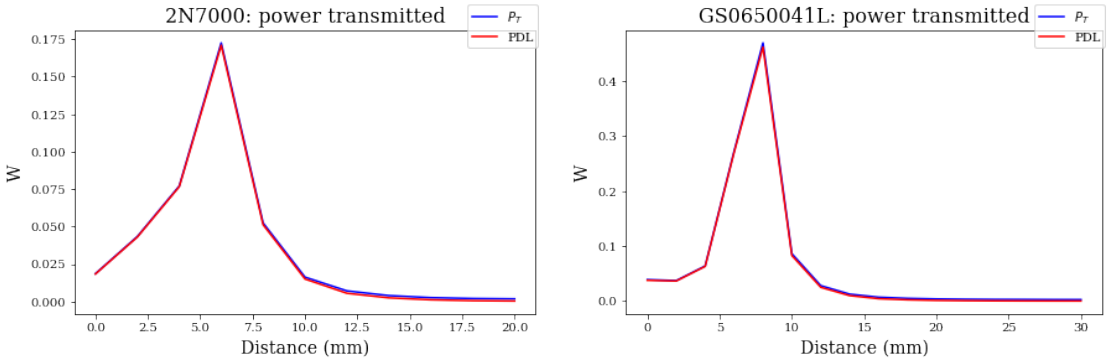

(a) 2N7000: P_T and PDL **(b)** GS0650041L: P_T and PDL

Figure 3.16: Transmitted power and Power delivered to the load in the two Class-E PA configurations

Even if the simulation results are coherent, a very high η_{LINK} in this range of distances, with K values minor than 0.1, seems unusual. This should be due to the simulation issues explained before and will be investigated later with proper PCB testing [Section 6.3].
The efficiency of more interest during the design of a WPT transmitter is η_{PA}; from Figure 3.17, it stays above a threshold of 75% from 6 mm to 10 mm, reaching a pick of 91% at 6 mm for the 2N7000 configuration; in the GS0650041L configuration, it stays above a threshold of 75% from 8 mm to 10 mm, reaching a peack of 88% at 8 mm. From previous observations on power waveforms varying the distance can be observed how they present a high pick focused in a narrow range of distances, centered at 6 mm, not aligned with the efficiency peak.

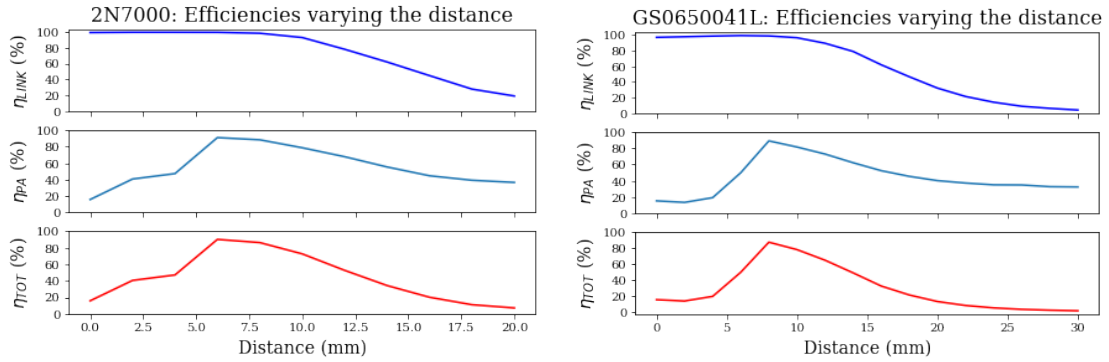

(a) Efficiency of the 2N7000 configuration **(b)** Efficiency of the GS0650041L configuration

Figure 3.17: Class-E PA efficiencies varying the distance between the coils

This behavior could be problematic in the real-world case when the distance between the transmitter and the receiver could vary by different millimeters.
Consequently, it is interesting to study how the power transmission could be incremented; the simplest solution is to increase the input voltage of the Power Amplifier, referring to ASK modulation [Sec. 2.6].

It can be observed that the transmitted power significantly increases by raising

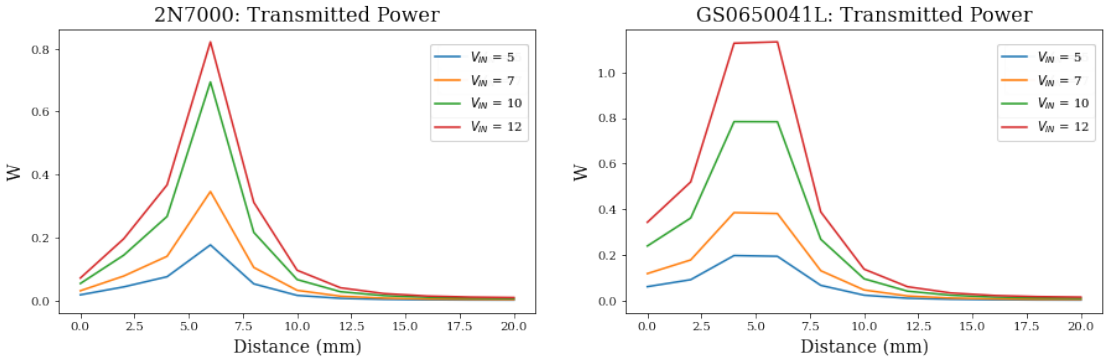

(a) 2N7000 P_T and PDL varying V_{IN} **(b)** GS0650041L P_T and PDL varying V_{IN}

Figure 3.18: Class-E PA P_T and PDL waveforms varying the input voltage

the input voltage [Fig. 3.18]. Meanwhile, the results of Figure 3.19 show that the efficiencies are not very influenced by these changes.

However, an excess of transmitted power could be problematic. To completely exploit this solution, a power management system should be designed; different possibilities have been explained before in section 2.6.

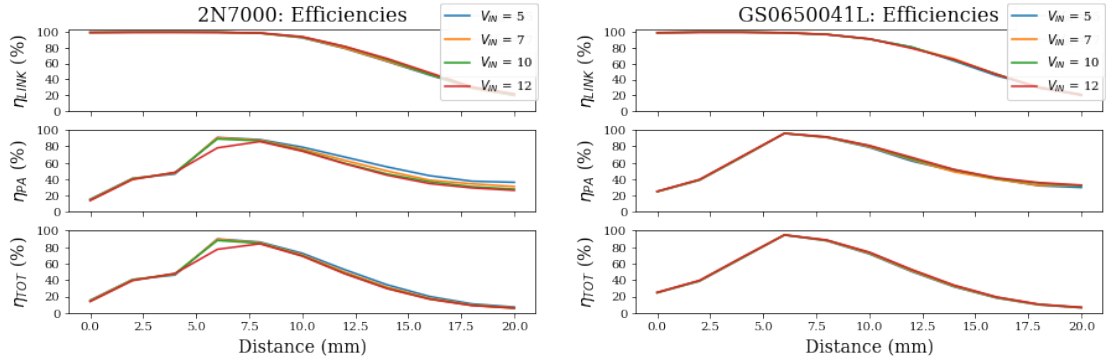

(a) 2N7000 efficiencies varying V_{IN} **(b)** GS0650041L efficiencies varying V_{IN}

Figure 3.19: Class-E PA efficiencies behavior varying the distance between the coils and the input voltage

In the actual case, the solution that gives enough power in the range of interest (from 6 mm to 10 mm) has been selected, respectively of 10V for both the 2N7000 and GS0650041L configurations, to guarantee more than 600 mW of power transferred.

3.3.4 Efficiency load variability

The most straightforward WPT Class-E PA schematic includes the receiver circuits and the inductive link component into the imaginary resistor R_{RXTX}. Being the resistor a passive component, we expect that by increasing its value, the dissipation of the circuits increases with a relative decrease in efficiency.
The link between the changes in R_{RXTX} with the distance and the load resulting from Equation 3.15 is shown in Figure 3.20. It can be observed how by increasing the distance the value of K_{RXTX} and R_{RXTX} decreases. The load R_L has a strong influence on the R_{RXTX} value.
Through the investigation of the dependence of efficiency from the value of the

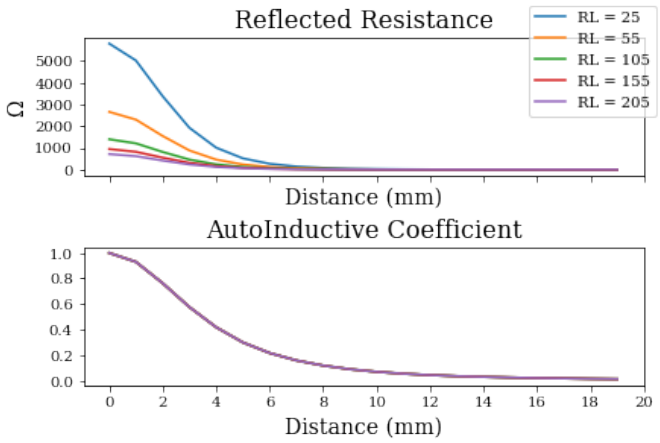

Figure 3.20: Relation of Ktxrx, R_{RXTX} with coil distance and load

load RL, varying both distance and load value on LTspice, it has been shown that the formulated considerations are correct. It could be observed how increasing the load value the efficiency grows rapidly for a specific distance range until a particular value, after which increasing the load causes an efficiency decrease. A range of load values, that allow the highest efficiency at the distances of interest, has been searched; for AIMDs, the range selected between 5 mm and 10 mm, and the highest efficiencies have been reached with a 150 Ω load value.

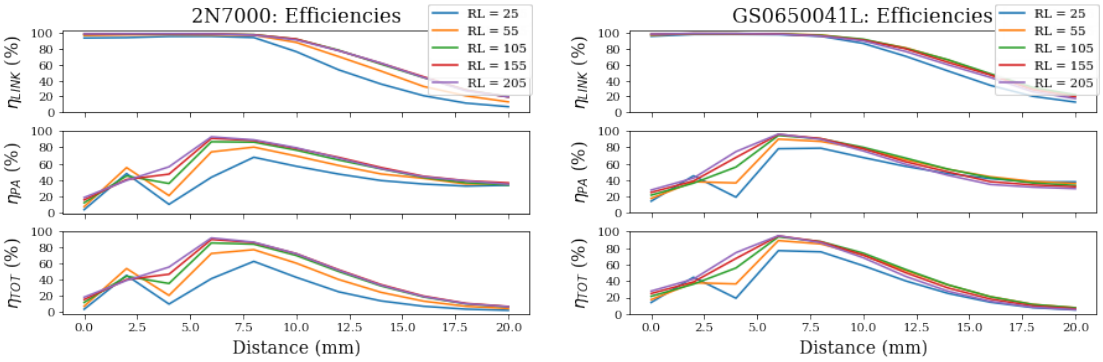

(a) 2N7000 efficiencies varying RL

(b) GS0650041L efficiencies varying RL

Figure 3.21: Class-E PA efficiencies varying the load

3.3.5 Final Class-E PA configuration

From the observation of the previous subsections, the final configurations have been selected, which will be tested with proper prototyping in the following chapters [Tab. 3.5].

Configuration	**L1**			**L2**			**L3**		
	L(μH)	Rp(Ω)	Cp(pF)	L(μH)	Rp(Ω)	Cp(pF)	L(μH)	Rp(Ω)	Cp(pF)
2N7000	40	0.18	0.11	4.5	0.38	9	4.5	0.38	9
GS0650041L	220	2.6	0.078	2.2	0.18	18	2.2	0.18	18
Configuration	**C1**		**C2**		**C3**		**Vin**	**RL**	
	C(pF)	Rp(pΩ)	C(pF)	Rp(pΩ)	C(pF)	Rp(pΩ)	(V)	R(Ω)	
2N7000	13	20	30	20	30	20	10	155	
GS0650041L	15	20	62	20	62	20	10	155	

Table 3.5: Final Class-E PA configurations with information about component, power voltage, and expected load

The configurations selected promise efficiencies and transmitted power as reported in Figure 3.22.

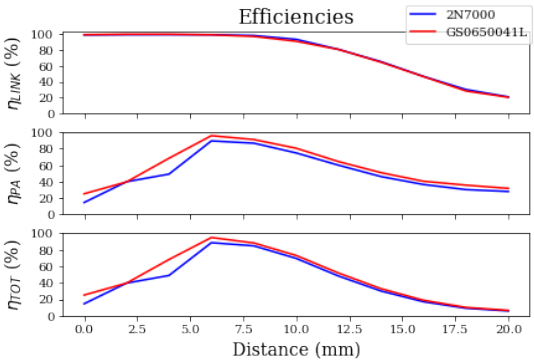

(a) Efficiency of 2N7000 and GS0650041L final configurations

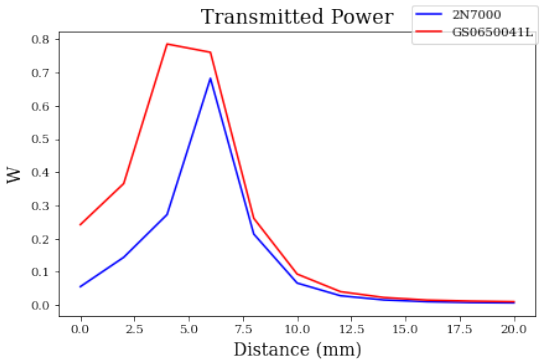

(b) Transmitted power by the 2N7000 and GS0650041L configurations

Figure 3.22: Efficiency and transmitted power comparison of the two final configurations obtained

From LTspice simulations, the key points of interest have been identified and will be extensively investigated during the prototype testing:

- Transistor drain voltage and current behavior
- Voltage and current measures for power estimation
- Influence of V_{IN} changes on the transmitted power behavior

Chapter 4

Preliminary Tests

The measurements of interest in Class-E PA have already been discussed [Chapter 3.3].
To measure powers, current and voltage measurements are needed, the quantities of interest are the transistor drain current, the current flowing in L2 and L3, and the voltage on C1, L2, RL and L3 [Fig. 4.1].

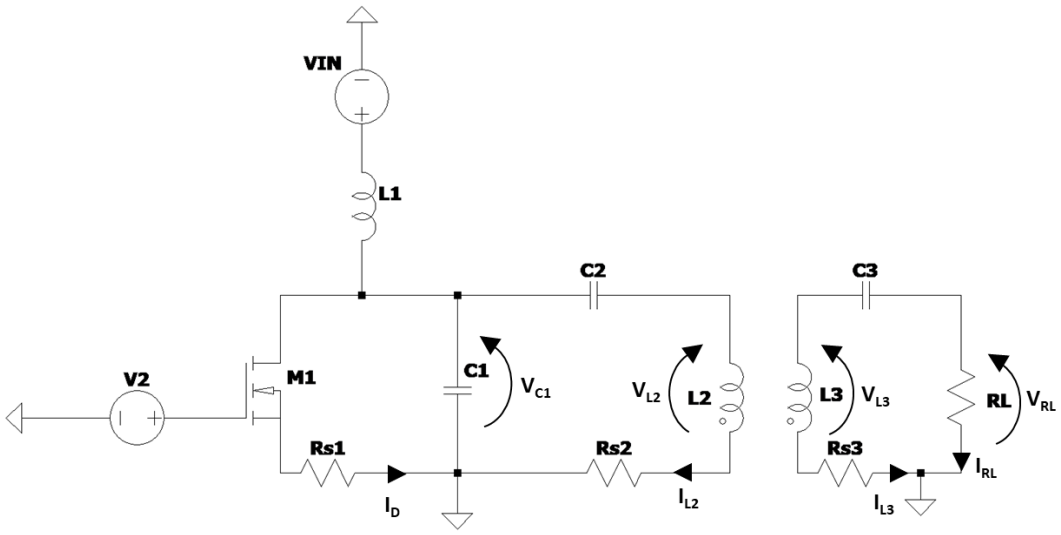

Figure 4.1: Quantities to be measured on the Class-E PA

Voltage measures could be easily obtained through an oscilloscope with proper characteristics; meanwhile, the current measures are more tricky; current measurements have been executed through resistive current sensing, which is thoroughly discussed in Section 4.2.

4.1 Voltage measurement

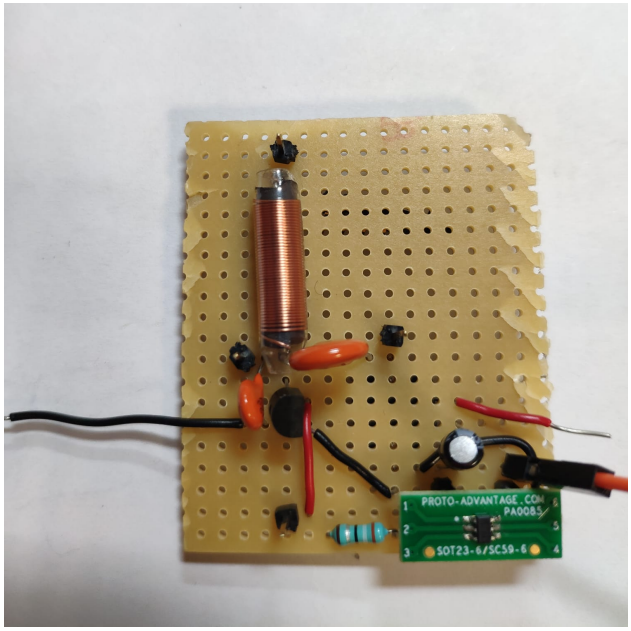

Figure 4.2: 2N7000 preliminary prototype on a welding breadboard

A prototype of the 2N7000 Class-E amplifier has been realized on a welding breadboard [Fig. 4.2], also a simple RLC receiver has been developed. Common multi-ceramic capacitors have been used, and the B8211E0000C023 power choke inductor has been selected. Tests on common breadboards were discarded due to high noise induced by parasitic capacitance, probably due to poor contacts.
Firstly, the transistor was tested. A square wave was applied on the gate, with an amplitude higher than the gate-to-source threshold, 6V, which is admissible by both transistors and guarantees the proper transistor function.
Generating a 13.56 MHz square wave could be difficult and proper equipment is needed: the Keithley 3390 with 25 MHz square wave bandwidth has been used.
In future perspectives, test equipment will not be used, making it more difficult to ensure the proper bandwidth. IC gate drivers have been investigated to assure a proper V_G even with lower bandwidth equipment.

4.1.1 Gate Driver

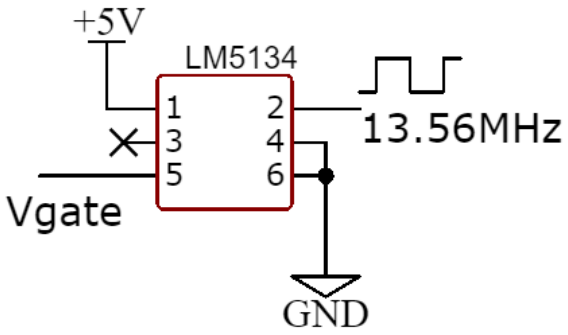

Figure 4.3: LM5134 settings

It is needed a fast gate driver that assures an output voltage higher than the gate-to-source threshold of the selected transistor. It must also supply enough current to the transistor gate; in fact, the parasitic capacitance C_{oss} of the transistor is equivalent to the load capacitance of the gate driver, so the current supplied must be high enough to guarantee the datasheet rise time.
The minimum output current of the driver could be calculated through the following equation:

$$I_{G(MIN)} = \frac{C_{iss} V_G}{t_{rise}} \tag{4.1}$$

Moreover, the gate driver must have a proper footprint to be used on a welding breadboard. The LM5134, standard SOT-23, with a rise time of 5 ns guaranteed by equation 4.1 has been selected. It has been used in the non-inverting mode with the following setting [Fig. 4.3]:

1. V_{DD} equal to 5 V
2. 13.56 MHz square wave input to IN
3. GND to INB
4. GND to Vss
5. floating PILOT
6. OUT to the transistor gate

A small gate resistance (10 Ω) on the output of the gate driver was selected to avoid transistor ringing and a high-value resistor (1 MΩ) to the ground was chosen to avoid the capacitive coupling driving the transistor.

4.1.2 Results

The following measures have been executed on the WPT prototype:

1. Voltages across the shunt capacitor C1 and the transistor gate
2. Voltage across the transmitter coil L2
3. Voltage across the receiver coil L3

Figure 4.4 shows the measure of VC1 compared to V_G, the results are similar to the simulation [Fig. 3.10].

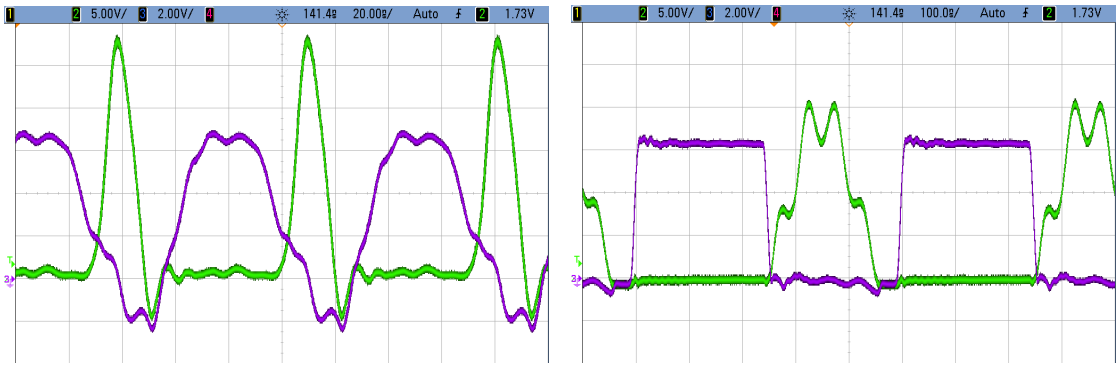

(a) Voltage across the shunt capacitor (VC1) with a 13.56 MHz input square wave

(b) Voltage across the shunt capacitor (VC1) with a 2 MHz input square wave

Figure 4.4: Comparison of VC1 and V_G with the input square wave at different frequencies

It should be clarified if the waveform oscillations are due to noise or improper transistor functioning. In RF, noise could easily be because of the parasitic capacitance induced by the breadboard's link. Reducing the frequency, the parasitic capacitance influences the behavior less, and the oscillation should decrease; it is observed in Figure 4.4b. Moreover, the violet waveform represents the generator square wave, and its oscillation supports the validity of the hypothesis; PCB results have solved the problematic [Fig. 6.4].

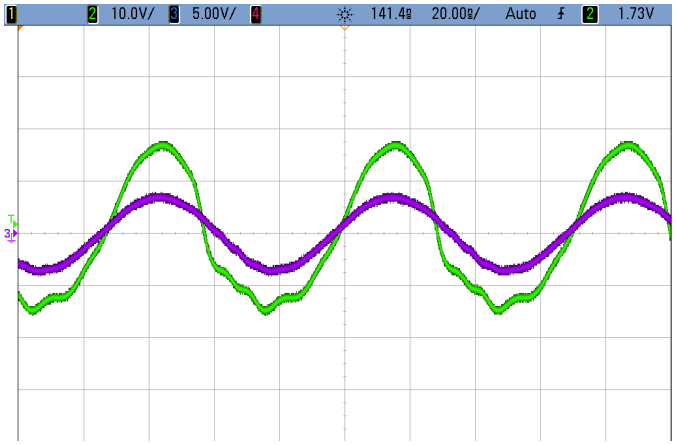

Figure 4.5: Waveforms measured across the transmitter and receiver coil

Figure 4.5 shows the voltages on L2 and L3, with a Tx-Rx distance equal to 3 mm; their behavior is similar to the simulation results, and the signal seems to be less affected by noise; a square wave, in fact, is more difficult to be measured than a sinusoid due to the fast rise edge. The MSO7104A oscilloscope, by Agilent Technologies, has been used for the voltage measurements.

4.2 RF Current Sensing

4.2.1 Background

Resistive current sensing is frequently used when dealing with low to moderate current levels [30]. It has three main possibilities: high-side, low-side and in-line measurements [Fig. 4.6].

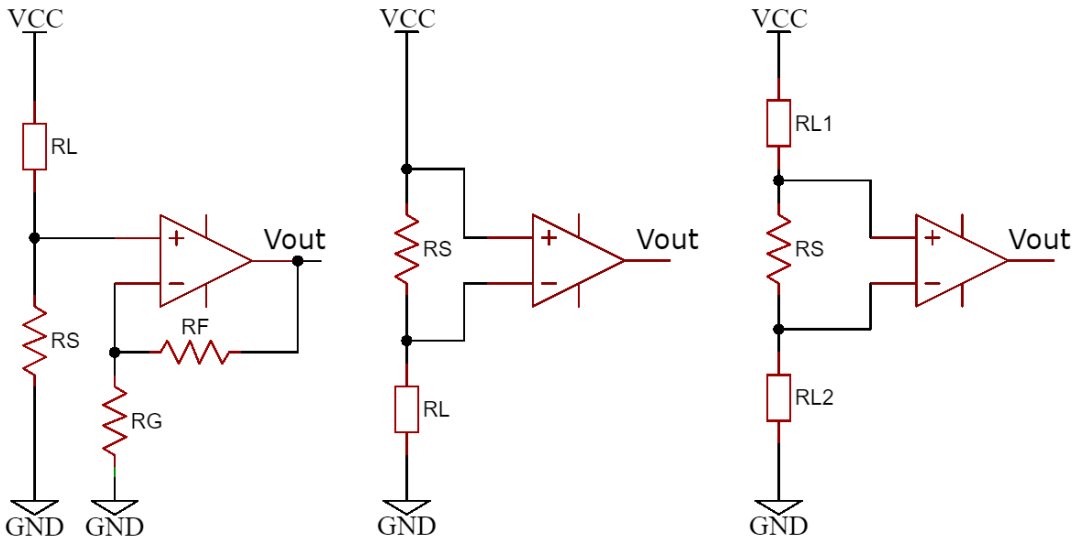

(a) Low-side **(b)** High-side **(c)** In-line

Figure 4.6: Resistive current sensing methods

High-side measurements have the current sense element connected between the supply bus and the load. This method can detect load short to the ground; the current is monitored directly from the source and has high immunity to ground disturbance. But, with high bus voltage, the availability of high-input common-mode voltage devices is limited.
Low-side measurements connect the current sense element between the load and the ground. This method is simple to implement and low cost; it has a wide range of available options, but it is difficult to detect load short to ground, and there could be system ground disturbance by the shunt resistor.
Lastly, In-Line measurements connect the current sense element between the loads. This technique allows true phase current at all times, reducing phase-to-phase errors. It has the best current feedback for the greatest accuracy. Disadvantages of this method are the PWM common-mode voltage and the high common-mode voltage combined with high dV/dT at the nodes of the shunt resistors.

When designing a current sensing circuit, it is necessary to choose the methodologies more suitable for the application. Afterward, the shunt resistor must be selected: it must not influence the circuit's behavior and have values usually in the range of (1 mΩ-100 mΩ).
Due to the low-value resistance, the voltage on the shunt resistor could be small and difficult to be read by the equipment. Consequentially, the voltage on the shunt resistor is usually amplified by a proper IC [31].
High-side and In-line measurements require a differential amplifier. Meanwhile, the low-side measurement could also be done with an Op-Amp.

4.2.2 Shunt resistor selection

In current measures, there is a trade-off between the measurement accuracy and the power dissipated by the shunt resistor [32]. In fact, by increasing the values of the shunt resistor, the voltage read by the equipment increases following Ohm's law:

$$V = RI \tag{4.2}$$

Higher voltages mean higher accuracy in the measurements. Anyway, increasing the resistance increase also the power dissipated, influencing the circuit behavior:

$$P = RI^2 \tag{4.3}$$

The correct trade-off has to be found. We could find the higher limit of the shunt resistor value through budgeting a maximum power dissipated, as follows:

$$R_{shunt} \leq \frac{P_{max}}{I^2_{load,max}} \tag{4.4}$$

The value of the shunt resistor could also be limited by the rail of the current sensing amplifier; the voltage on Rs must not exceed the positive rail voltage.

$$R_{shunt} \leq \frac{V_{out,max}}{I_{load_max} A_d} \tag{4.5}$$

On the contrary, the lower limit of the shunt resistor could be found by the negative rail of the current sense amplifier.

$$R_{shunt} \geq \frac{V_{out,min}}{I_{load_min} A_d} \tag{4.6}$$

From LTspice simulations, both the currents across L2 and the transistor drain do not overcome 200 mA. Initially, due to the small values of current to be measured, a shunt resistor value of 100 mΩ generating a voltage of 15 mV, has been chosen. Hypotisizing common rail of ±5 V, with the value of the shunt resistor selected, the current measures stay in the range imposed by Equations 4.6,4.5 if the amplifier gain does not exceed 250.

4.2.3 Current sensing amplifier selection

In order to select a current sensing amplifier the following characteristics must be analyzed:

- Typology: Differential or operational amplifier
- Input offset voltage, it can be corrected, but it is better if small
- Input offset current
- Input Bias current
- Gain Bandwidth Product (GBW), index of maximum gain admissible given the bandwidth
- Input Voltage Noise, noise variable with frequency
- Input Current Noise, noise variable with frequency
- V_{DD}, single or dual

The amplifier, to properly function, needs a bandwidth one order of magnitude higher than the carrier frequency (100 MHz). Differential amplifier solutions with this bandwidth have not been found on the market. Meanwhile, there are many Op-Amp available options.
For simplicity, knowing the current waveform to be measured, the amplifier must be dual. Regarding the GBW, solutions with less than 2 GHz of GBW, resulting in the minimum gain achievable of 20 considering a 100 MHz bandwidth, have not been investigated. The different noise contributions must be at least one order of magnitude lower than the relative expected quantities of input and output.
The OPA847, a 3.9 GHz GBW Op-Amp with stable gains higher than 12, was selected.

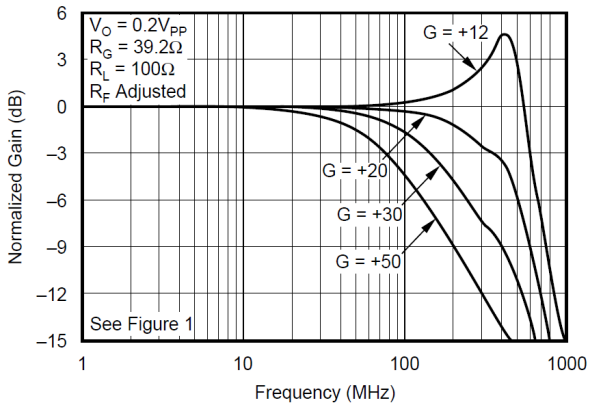

Figure 4.7: OPA847: Gain behavior varying the frequency

The datasheet [Fig. 4.7] illustrates how the maximum Gain admissible for our application is 20. To obtain a Gain equal to 20, the setup presented in Figure 4.8 has been chosen. The capacitors on the two rails are needed to reduce power noise. Meanwhile, RF and RG have been designed as follows:

$$Ad = 1 + \frac{RF}{RG} \tag{4.7}$$

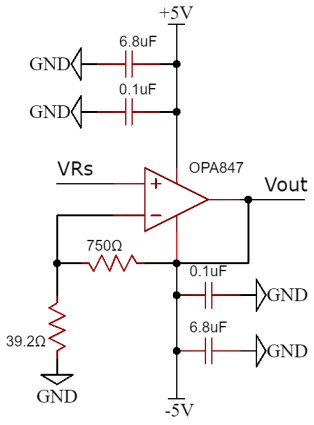

Figure 4.8: OPA847 setting

4.2.4 Preliminary current sensing circuit test

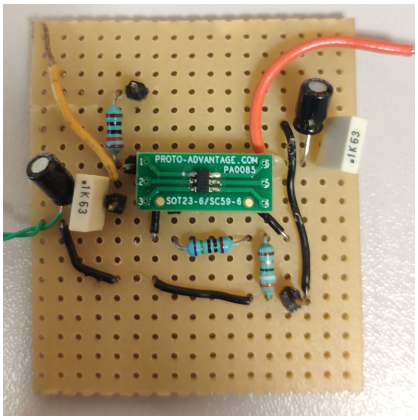

Figure 4.9: OPA847 prototype on a welding breadboard

The OPA847 has been initially tested on a welding breadboard [Fig. 4.9]. An overlap of a higher frequency sinusoid is observed [Fig. 4.10] by measuring the output voltage with a 100mVpp input sinusoid.

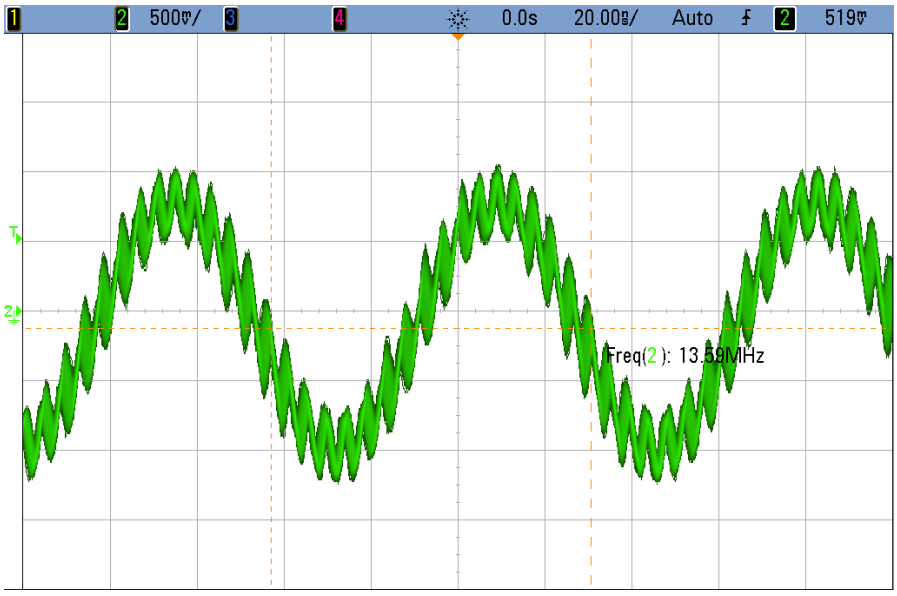

Figure 4.10: OPA847 output voltage with a 200 mVpp input sinusoid

A possible explanation for this phenomenon is the instability of the amplifier. STMicroelectronics reports how [33], working with a capacitive load, the amplifier could be unstable and show a behavior comparable with our tests. In our application, there is no actual capacitor, but the capacitive load could be constituted of the parasitic capacitance of the oscilloscope probe, equal to 12 pF.
A possible solution is applying a compensation method to stabilize the solution. In particular, the method named out of the loop [33], adds a resistor in the output series. This resistor, combined with the capacitive load (in our case, the probe capacitance), forms an RC filter, increasing the stability but reducing the bandwidth, which has to be correctly designed.
The oscilloscope data have been imported into Python. It was observed, looking at the PSD of the signals with different input sinusoids, how the high-frequency noise component changes with the frequency, not being fixed to a specific frequency.

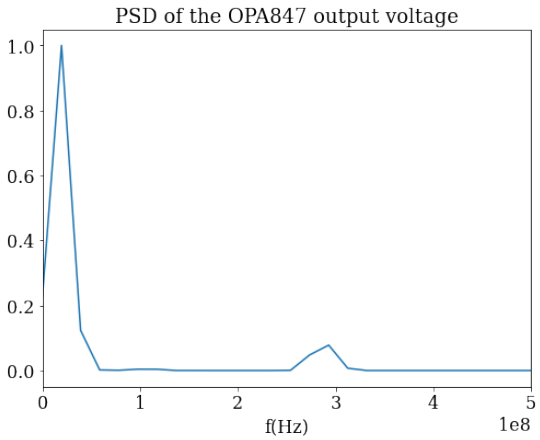

(a) PSD of the OPA output voltage with a 13.56 MHz input sinusoid

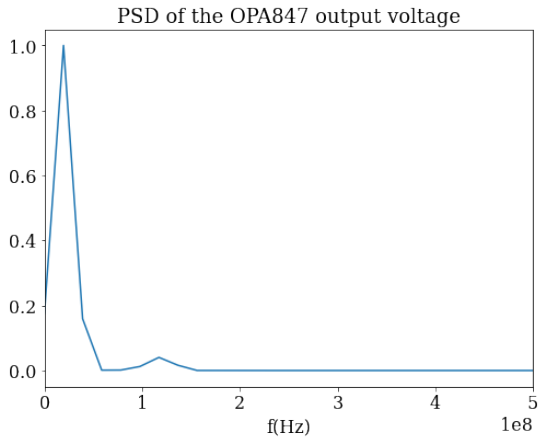

(b) PSD of the OPA output voltage with a 25 MHz input sinusoid

Figure 4.11: PSD of the OPA847 output voltage varying the frequency of the input sinusoid

A hypothesis on the origin of this instability could be the resistors, we are using simple breadboard resistors working in the RF range, and the value of these resistors could become unstable, contributing to the instability of the system.
Thus, the resistors have been tested with the Agilent 4294A Impedance Analyzer from DC to 110 MHz. Once analysed both resistors, the results show how even if the resistor values change, their ratio stays similar to twenty up to 30 MHz [Tab. 4.1]; consequentially, the output voltage has the expected amplitude, but the resistor value variation could result in instability.

f(Hz)	ϕ (°)	Z(Ω)	ReZ	ImZ	ϕ(°)	Z(Ω)	ReZ	ImZ	Gain	
		39Ω				**750Ω**			**Module**	**Phase (°)**
1k	-0,0965	38,91	38,90994	-0,06553	-0,09868	747,8	747,7989	-1,28793	20,2	0
13.7M	-19,74	150,88	142,0135	-50,9601	38,86	2440	1899,983	1530,904	16,7	55,6
20.34M	-120,94	40,74	-20,9461	-34,9429	-172,13	809,5	-801,876	-110,842	20,5	-49
30.69M	144,97	11,44	-9,36766	6,56662	137,02	12,2	-8,92542	8,317265	2,1	-62,2
50.41M	-49,55	9,65	6,260768	-7,34338	-139,25	18,5	-14,015	-12,0761	2,0	-4,1

Table 4.1: Op-Amp Resistor analysis of Impedance varying the frequency

Therefore, current measures were inoperable; two different strategies were formulated in order to solve the problem with the PCB prototype: buying RF resistors with value stable until GHz and checking if there are improvements in the output; foreseeing the out-of-the-loop compensation method adding a resistor in series on the amplifier output; in case it is useless, a 0 Ω resistor could be put.
If filtering is needed, the design must be done accurately; in our application, we are interested in the measurement of current in two nodes, the transistor drain, and L2; from simulation, I_D is expected to have different frequency contributes, rapid rise edge, which could make difficult to find the appropriate cut frequency. Meanwhile, I_{L2} is expected to be sinusoidal, specifically at 13.56 MHz. The Class-E PA has been simulated on Xyce, a spice-compatible electronic circuit simulator, to observe the frequency component of the system. Observing the behavior of the first 10 harmonics (both on the positive and negative side), I_{L2} could be considered a pure sinusoid at 13.56 MHz, due to the second harmonic difference of 42dB compared with the firsts. Figure 4.12 shows the modulus and phase of the current across L2, the horizontal label shows the frequency, centered in 0 at the carrier frequency (13.56 MHz).

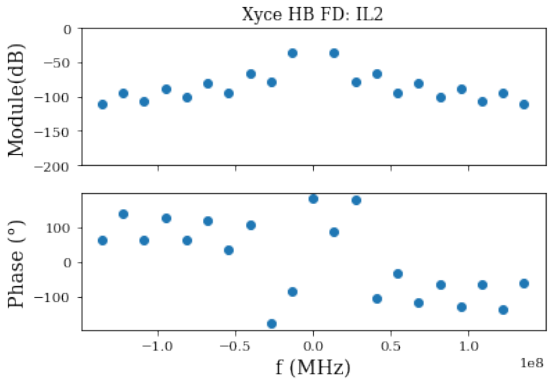

Figure 4.12: Xyce frequency study on the coil current waveform

Chapter 5

PCB design

The PCB was designed through Altium Design, a PCB software design leader which combines schematic and layout editors.
During the design of a PCB it is necessary to follow different steps; firslty, the library components must be selected and eventually imported for designing the schematic. Secondly, the PCB layout will be generated from the schematic, all the components are imported into an apposite software tool, and the designer has to define the rooting and other design choices, which will be discussed later.

5.1 RF constraints

RF PCB design has several constraints to reduce noise as much as possible; they coud be summarized in twelve points [34, 35]:

1. Straight PCB wires with 45° corners, the fewer corners, the better
2. Avoid using vias to connect components
3. PCB wires should be short
4. Make parallel wires short and leave enough distance between them
5. Use ground lines around the clock line; make the clock line perpendicular to the main signal line
6. Avoid loops for high-frequency PCB wires
7. Use inner middle layers as power and ground layers
8. Use perpendicular PCB wires between the two adjacent layers
9. Separate ground lines of analog and digital signals

10. Separate the power supply of digital and analog signals
11. Add one high-frequency decoupling capacitor to each of the IC block's power supply pin
12. Increasing the high-frequency decoupling capacitance of the power pins of IC block

The design of the PCB lines could be critical. Being lines of conductors, they have their parasitics, and their size must be limited depending on the frequency of use. To help the designer during RF PCB design, Avago Technologies provides AppCAD, an RF design software, free of charge.

5.2 Schematic

The choice of the coil, transistor, and current sense amplifier has already been explained respectively in Sections 3.1.1, 3.1.4, 4.2.3. The other component choices are presented in the following section.

5.2.1 Gate Driver

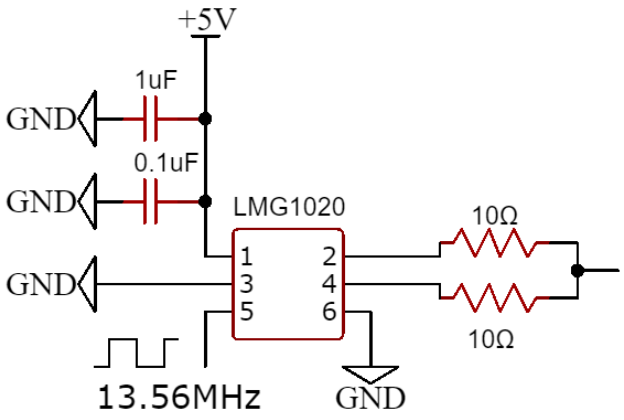

Figure 5.1: LMG1020 settings

In Section 4.1.1 the steps to be followed when choosing a Gate Driver were explained, and the LM5134 was selected. This Gate Driver was chosen to be used on a breadboard.
While looking for other solutions on the market without this limitation, the BGA (Ball grid array) LMG1020 was found; it is faster and smaller than the previous

choice. The LMG1020 [Fig. 5.1] has been set in the non-inverting mode, the not used pin IN- was connected to ground. The two output pins were arranged with a gate resistor on both of them and were connected before reaching the gate transistor pin.

5.2.2 Choke Power Inductor

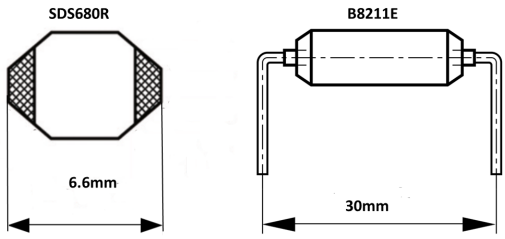

Figure 5.2: B8211E and SD680R power choke inductor sizes

The B82111E previously selected [Section 4.1] is available with different inductance values that satisfy the requirements. The SDS680R has also been selected, which is SMD, smaller[Fig. 5.2], and useful in future perspective for an AIMDs application.
The components selected are compared in Table 5.1.

Model	L(μH)	SRF(MHz)	Rp(Ω)	Tol. (%)	Imax(A)
B8211E0000C023	40	90	0.18	20	2
B8211E0000C026	220	32	2.6	20	0.5
SDS680R-473M	47	20	0.230	20	0.5

Table 5.1: Comparison of different Power Choke Inductors

The PCB has been arranged to test both B8211E and SDS680R; if they do not influence the performance, the latter would be prioritized.

5.2.3 Capacitors and Resistors

The choice of capacitors could be divided into two groups: the RF capacitors, respectively C1 and C2, and the decoupling capacitors. Regarding C1 and C2, they have more limitations: their SRF (self-resonant frequency), must be higher than 50 MHz, and their class should be the cg0. The decoupling capacitors are used to decouple the power line from the circuits, avoiding possible noise. It was chosen to put two capacitors, respectively of 0.1 µF and of 10 µF, on the main power line.
Other decoupling capacitors have been placed on the Gate Driver and the Current sensing amplifiers following the indication on the datasheet: respectively, two capacitors of 1 µF and 0.1 µF for the LMG1020 and two capacitors of 6.8 µF and 0.1 µF for each OPA847.
The resistors used on the LMG1020 output have an SRF minimum of 50 MHz. Meanwhile, all the OPA847 resistors, due to the instability problem, have been chosen with an SRF of GHz; resistance values of 25 Ω and 500 Ω have been chosen to guarantee a Gain of 20.

5.2.4 Thermistor

In AIMDs, it is important to check the coil temperature. Although the coil temperature is less important on the transmitter side than on the receiver side, it has been evaluated equally. Being the coil selected SMD, a flexible ultra-thin thermistor has been selected, the 103-JT-025. Its sensitive part is only 0.5 mm thick and could be positioned under the coil.

Following the same precautions, also the receiver schematic has been designed. The resulting schematics are shown in Figures 5.3, 5.4, 5.5.

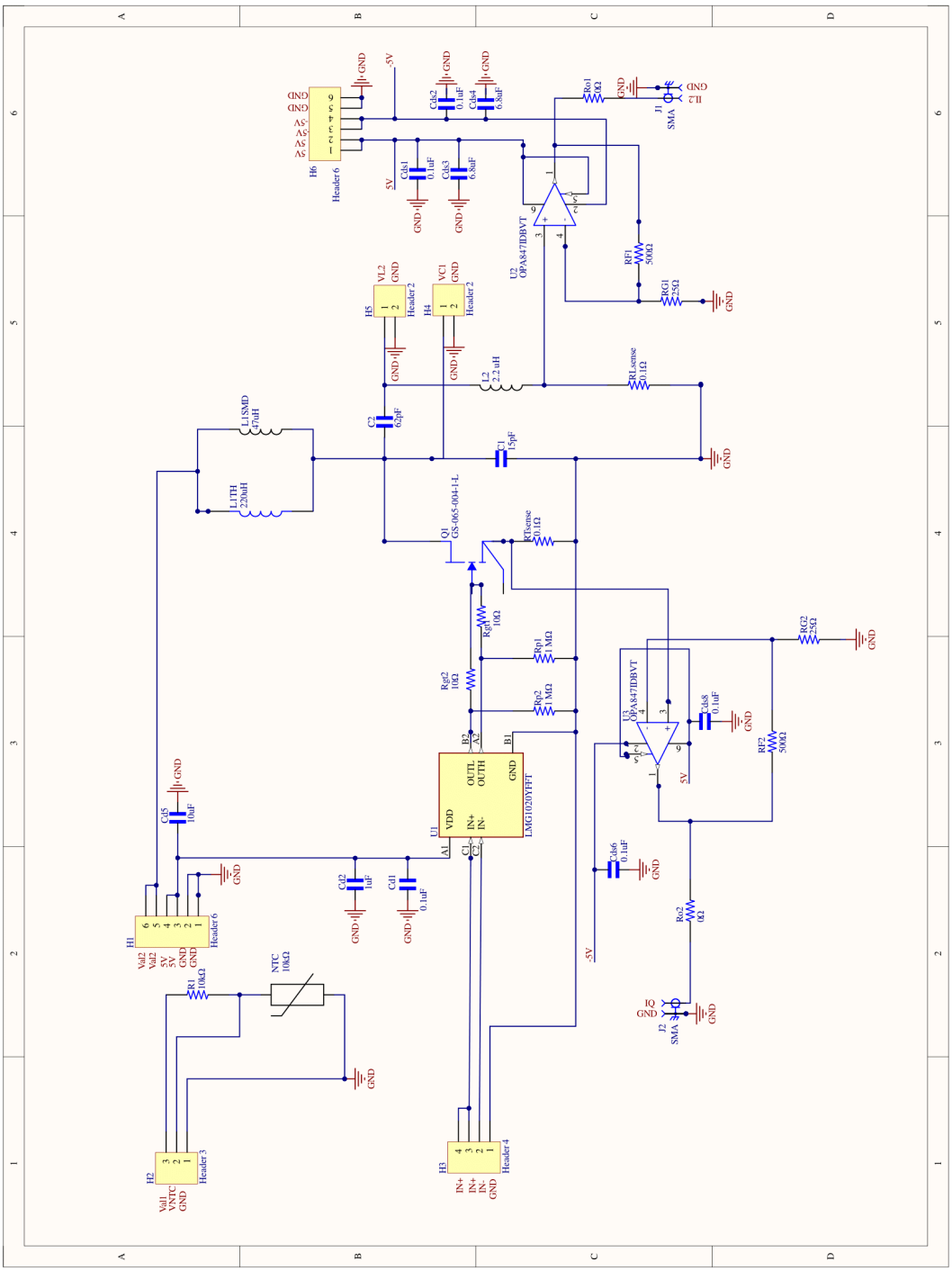

Figure 5.3: Altium schematic of the GS0650041L configuration (AIMD HF IPT TX PA v02a)

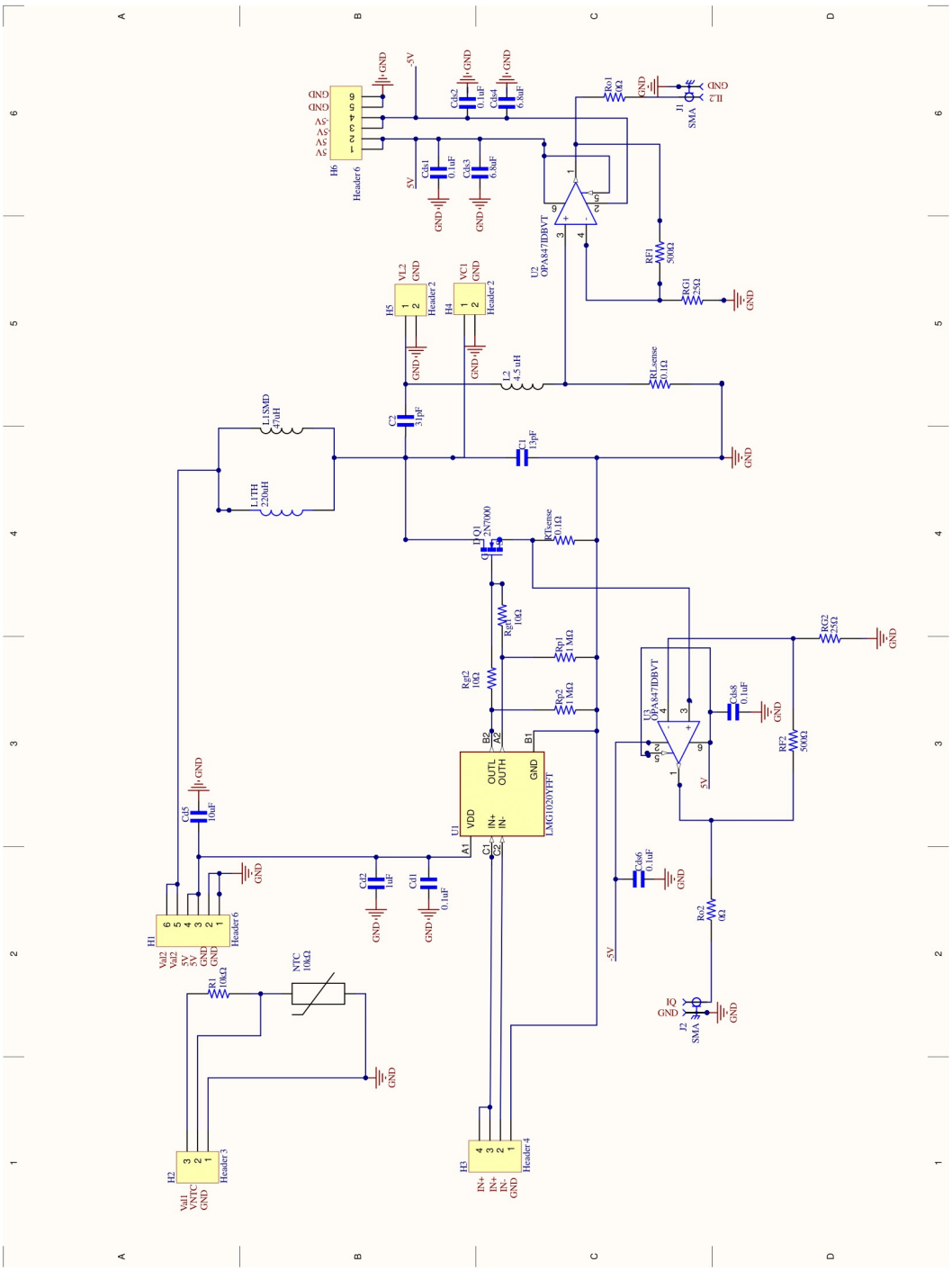

Figure 5.4: Altium schematic of the 2N7000 configuration (AIMD HF IPT TX PA v02b)

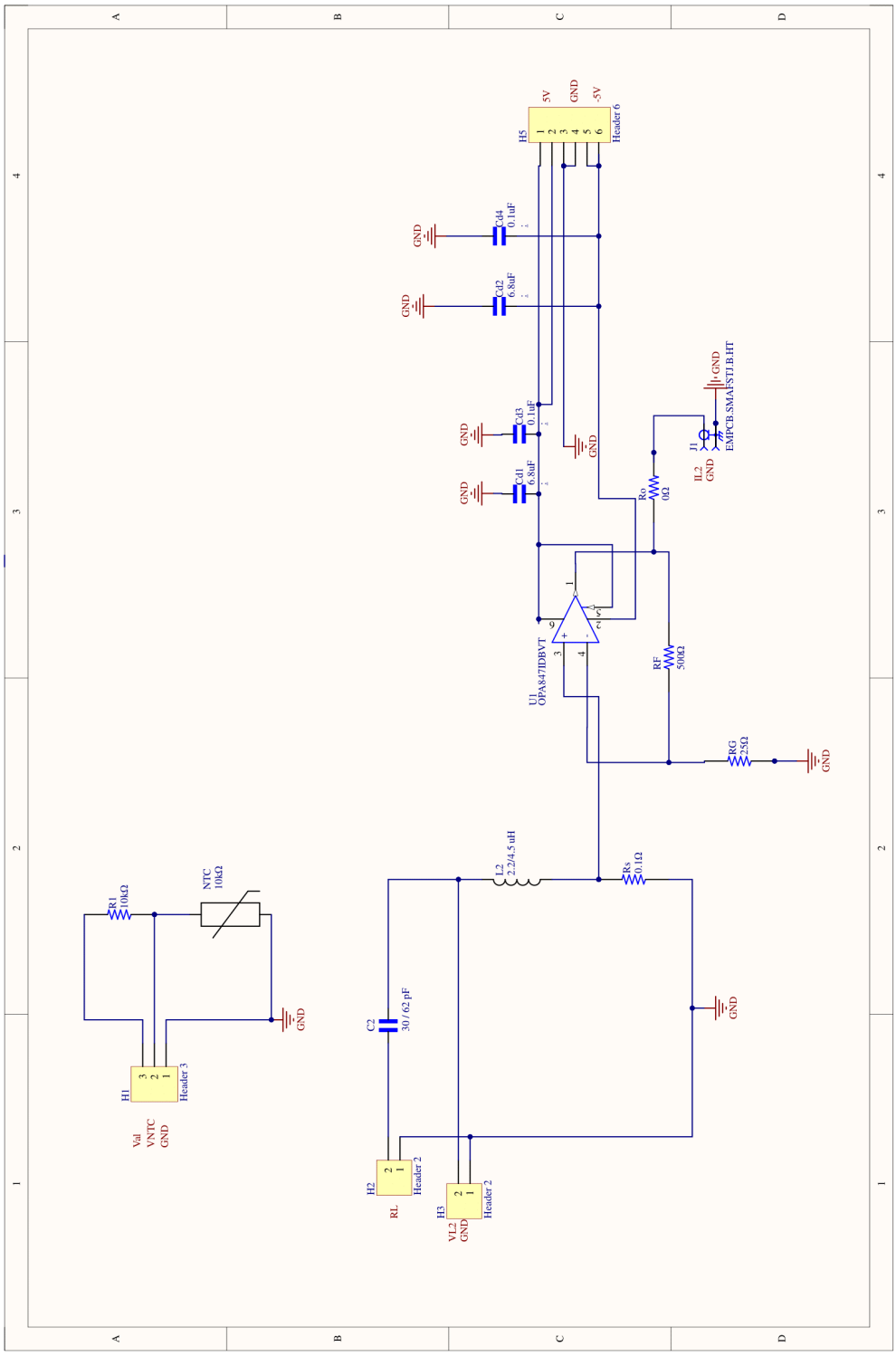

Figure 5.5: Altium schematic of the receiver (AIMD HF IPT RX PA v02)

5.3 PCB layout

The final PCB layout of the two configurations is shown in Figure 5.6, 5.7, 5.8

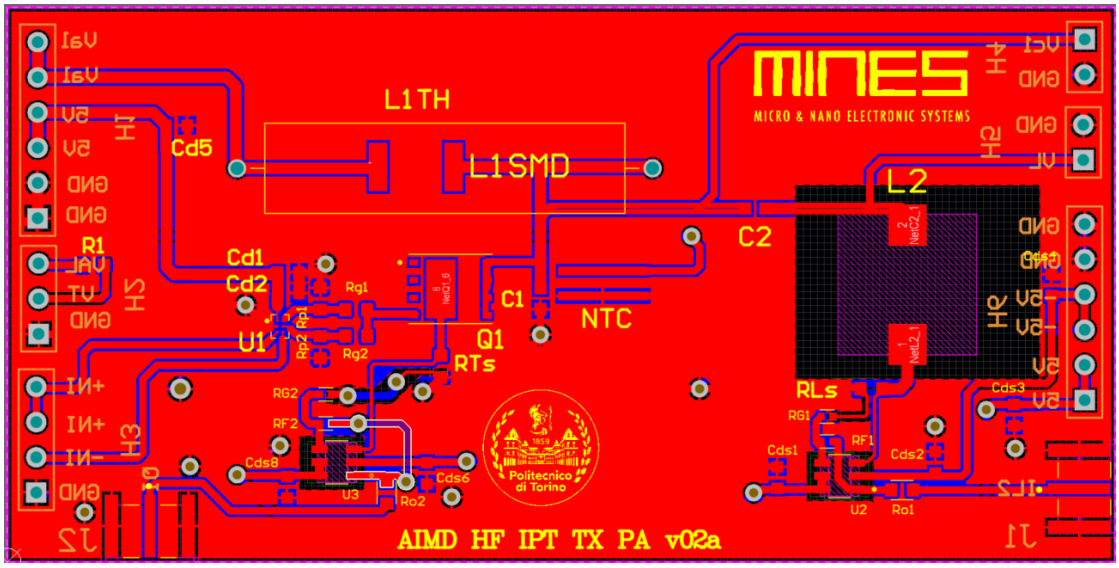

(a) AIMD HF IPT TX PA v02a top layer

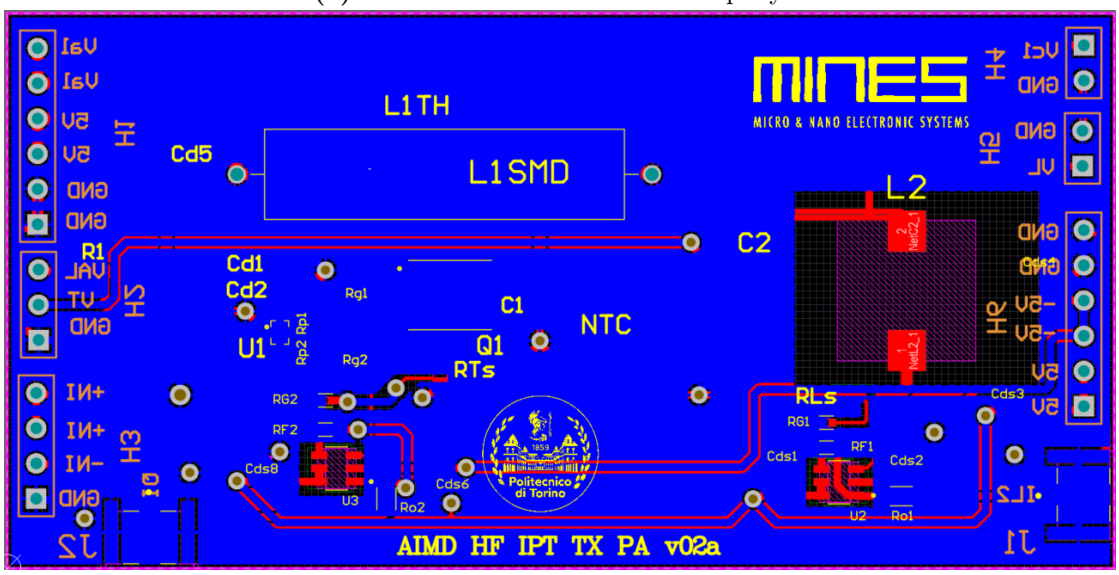

(b) AIMD HF IPT TX PA v02a bottom layer

Figure 5.6: AIMD HF IPT TX PA v02a PCB layout

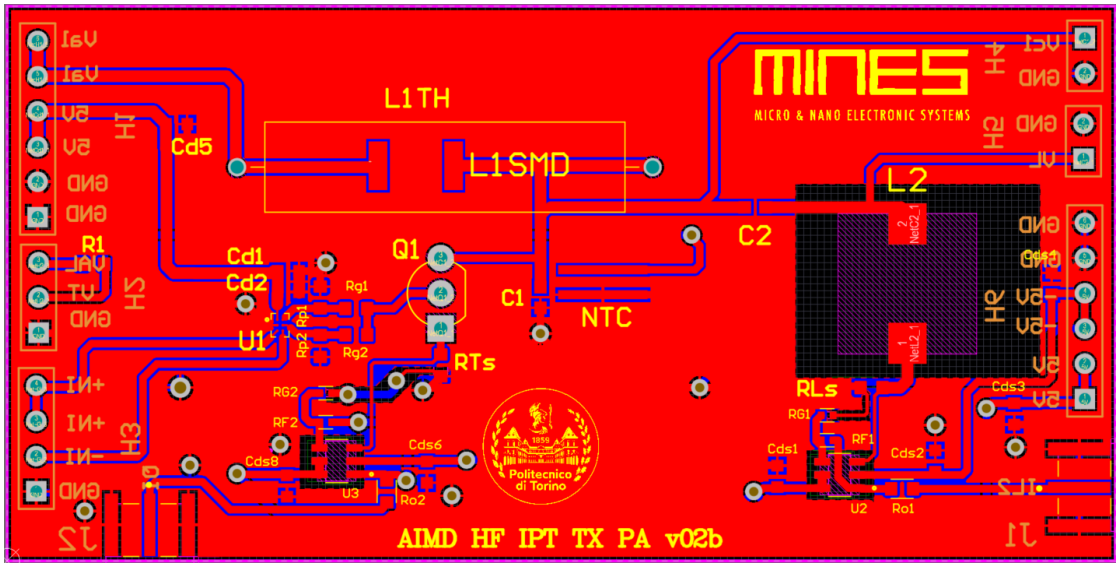

(a) AIMD HF IPT TX PA v02b top layer

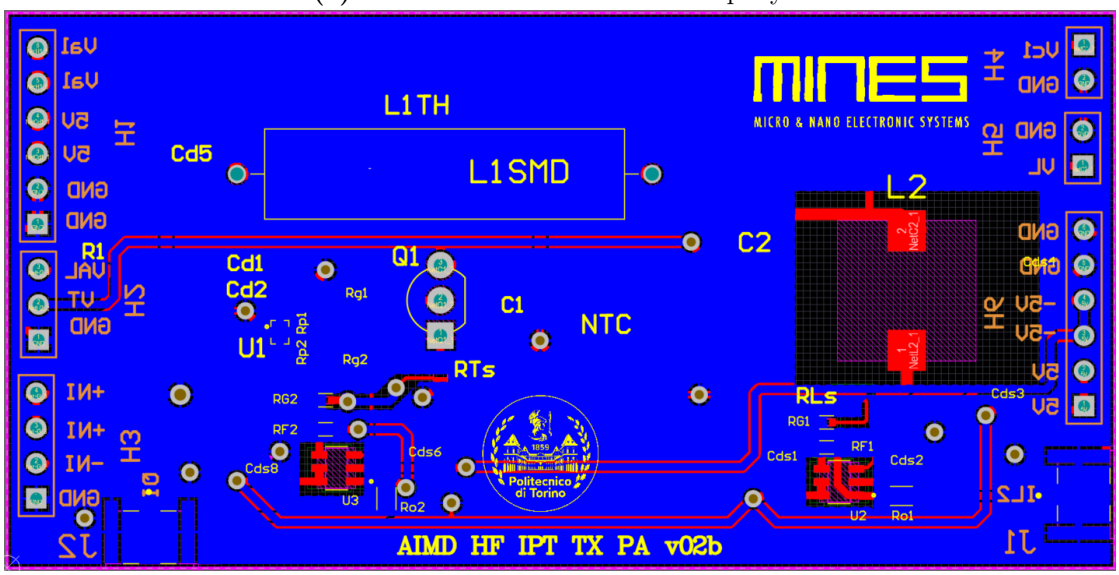

(b) AIMD HF IPT TX PA v02b bottom layer

Figure 5.7: AIMD HF IPT TX PA v02b PCB layout

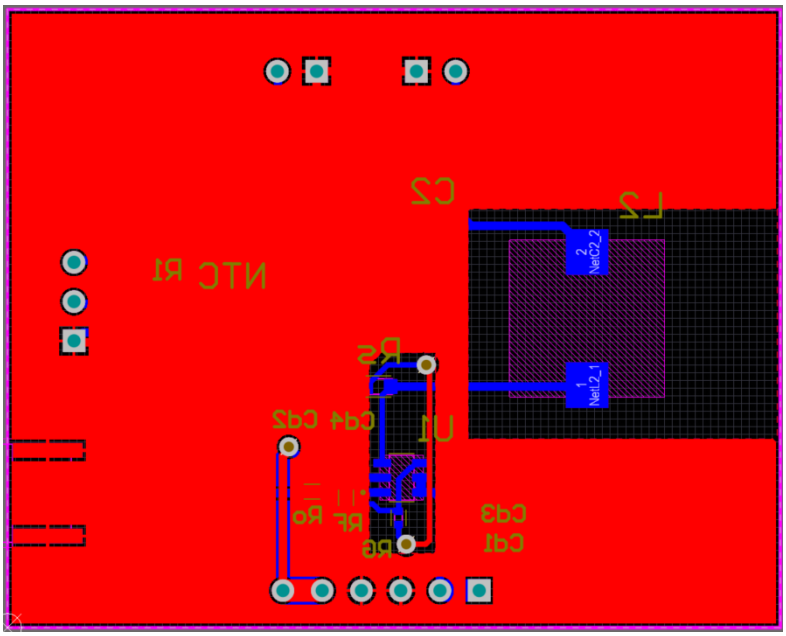

(a) AIMD HF IPT TX PA v02 top layer

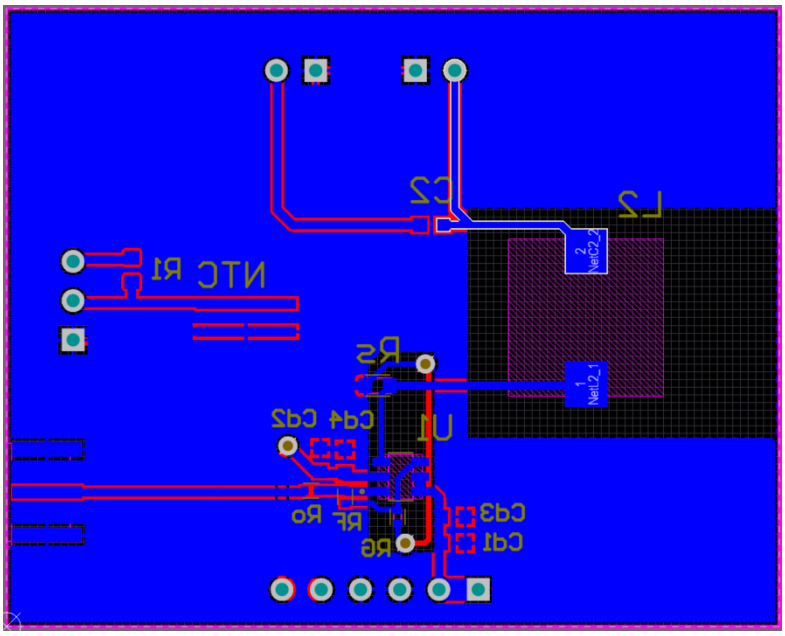

(b) AIMD HF IPT RX PA v02 bottom layer

Figure 5.8: AIMD HF IPT RX PA v02 PCB layout

The transmitter PCB size are 80 mm · 40 mm; at this moment, it is important to prove the system's functioning. In the future, the size must be reduced. Being aware of that, the PCB has been designed with consciousness: the major components are in the center of the PCB; if the current sensing subcircuits are not considered, the Class-E PA sizes are 55 mm*22 mm. After the evaluation of the prototype, the current sensing subcircuits will not be necessary anymore.
The receiver PCB is 40 mm*40 mm; the coil has been positioned at the same point, specularly on the Tx and Rx, to make tests faster and easier.
The size of the routes is different in the PCB: the RF and power lines have been designed larger; moreover, it has been chosen to put a ground layer on both the top and the bottom layer.
A cutout in the ground layers has been opened in the coil areas to avoid electromagnetic issues; the ground layer is a large area of conductive material, and it can act as a magnetic shield, affecting the performance of the system [10].
The usage of vias was limited where possible in the RF lines, following the rules previously cited.
Appcad has been used to ensure that the size and length of the routes respect the constraints. The following sections discuss in detail the design choices for each component of the transmitter circuit.

5.3.1 Headers

Right angle headers have been selected, positioned on the smaller side only, to facilitate the usage of the testbench developed, discussed later [Section 6.1]. An SMA adapter is used for each OPA847 output, increasing the robustness of the system to noise.
For a simpler usage of the equipment, two headers were provided with each crocodile clip.

5.3.2 Transistor and Gate driver

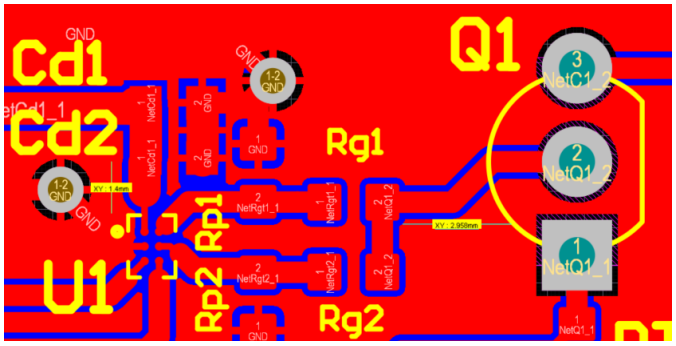

Figure 5.9: PCB layout of the transistor (Q1) and gate driver (U1)

The LMG1020 (U1) setup has been designed as suggested on the datasheet [Fig. 5.9]; the two decoupling capacitors Cd1 (1 µF) and Cd2 (0.1 µF) are positioned near the power pin (1.5 mm). Additionally, the gate resistors Rg1 and Rg2 are positioned as close as possible to both the transistor (Q1) and the gate driver (maximum distance of 3 mm).

5.3.3 Choke Power Inductor

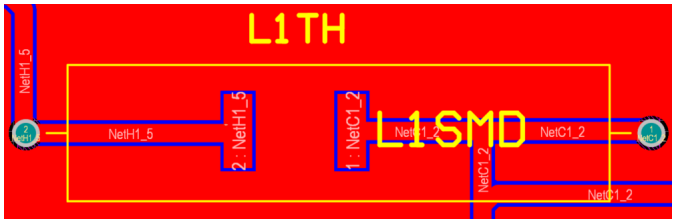

Figure 5.10: PCB layout of the power choke inductors

As previously discussed, there are two possible choices of choke; both choices are provided for further investigation. To save space, the two chokes are positioned one above the other; the SDS680R library was not available on the web and was designed by the datasheet.

5.3.4 RLC circuit and Thermistor

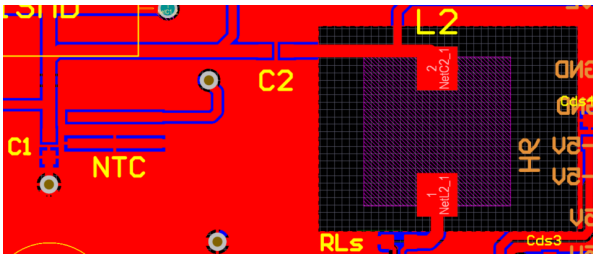

Figure 5.11: PCB layout of the RLC subcircuit

The RLC circuit was made as small as possible, with the size constraints imposed by the thermistor, which must be 25 mm from the coil to be positioned under it. The thermistor library was not available on the web and was designed by the datasheet.

5.3.5 Current sense amplifiers

The OPA847 setup was done as suggested on the datasheet: the distance from the 0.1 µF decoupling capacitor is less than 0.25«, meanwhile, the 6.8 µF capacitor is positioned at a higher distance, and it is in common between the two amplifiers. A window in the ground layer around the amplifiers has been opened to avoid unwanted capacitance. The feedback and series resistors have been positioned as close as possible to the amplifier to reduce parasitic capacitances [Fig. 5.12].
To improve measures accuracy, the input and ground voltages are taken from the inner pad of the shunt resistor; the ground of the two OPA847 is divided from the poor ground layer.

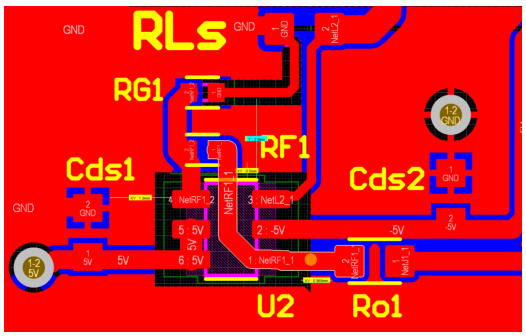

(a) PCB layout of the coil current sensing amplifiers

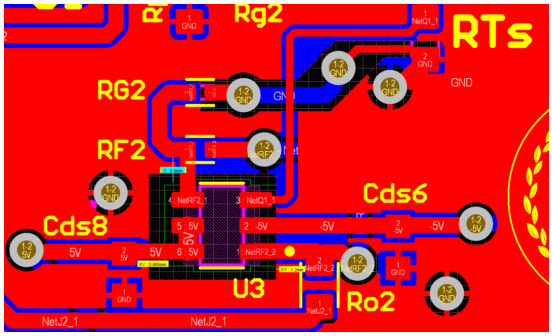

(b) PCB layout of the transistor current sensing amplifiers

Figure 5.12: PCB layout of the current sensing amplifiers PCB section

Chapter 6

System performance analysis

Once designed and produced, the PCB prototypes must be tested to compare the results with the simulation. With LTspice, there was the possibility to test the performance variation with distance through the auto inductance coefficient variation.
In AIMDs, there could be variations in angle, misalignment, and distance. For a thorough investigation, a testbench with three Degrees of Freedom (DoF) has been realized. It permits millimetric control of these parameters during the tests; specifically, the distance and the misalignment have been tested from 0 mm to 20 mm, while the angle has been tested from 0° to 3°.

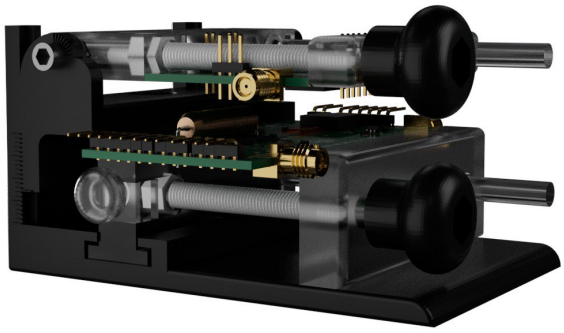

Figure 6.1: 3D printed testbench

The types of equipment used to evaluate the circuit performance are a DC power supply, an oscilloscope, a waveform generator, and a microcontroller board. Specifically, the setup of Figure 6.2 has been implemented.

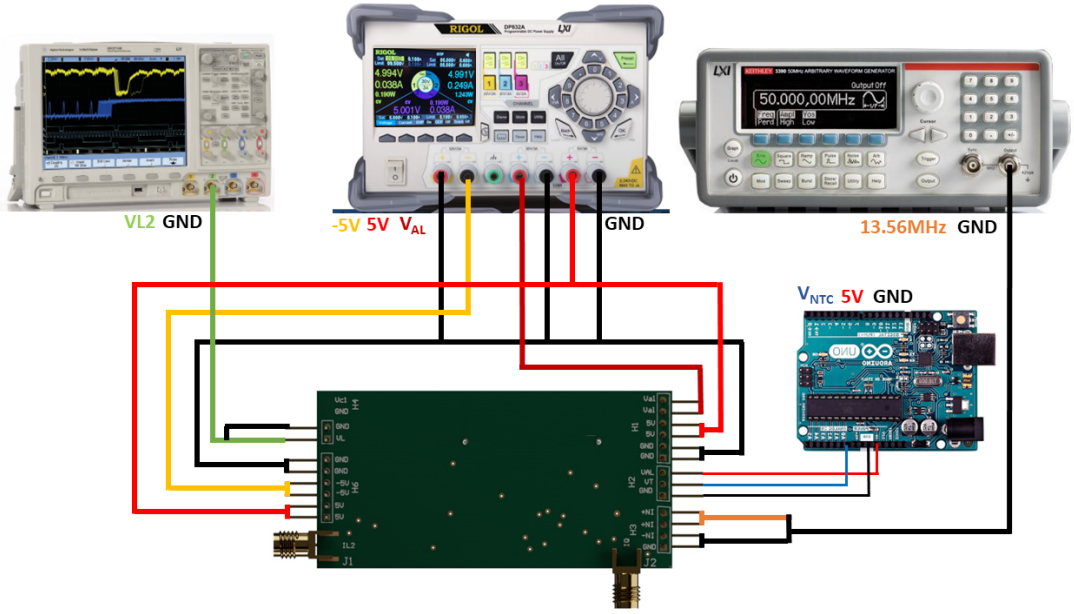

Figure 6.2: Measurement setup

The DC power supply powers the current sensing subcircuits with a dual power supply through channels 1 and 3, the 5 V channel powers also the LMG1020; the Class-E PA is powered by channel 2. The waveform generator output is a 13.56 MHz square wave defined with 6 V high level, 0 V low level, and 50% DC. The oscilloscope uses passive probes for voltage measurements and BNC to SMA probes for current measurements. The microcontroller board is needed to power and read the thermistor measures; an Arduino UNO has been used in this study. Initially, the current consumptions have been analyzed; channel 1 consumes 83 mA while channel 3 consumes 38 mA, as expected from the OPA847 and the LMG1020 operating currents, respectively of 19 mA and 45 mA. The average consumption of channel 2 depends on the status of the WPT system and will be thoroughly studied in the following section.

6.1 Testbench

The testbench realized was 3D printed by the FORM3 resin printer; it is composed of seventeen components; plastic bolts have been used to avoid electromagnetic issues during WPT system testing. Two clamps lock the transmitter and the receiver, this mechanism allows the reuse of this system with PCBs of different sizes.
To change the distance, the clamps of the receiver are connected to the docking station through a shaft that changes its height through a bolt [Fig. 6.3a].
Regarding the angle, two bolts connect the shaft to the clamp; if they are unscrewed, the angle could be changed [Fig. 6.3b].
Lastly, for misalignment variations, the transmitter clamp has a slide mechanism on the docking station [Fig. 6.3c]. For each DoF, a rule has been printed on the relative part to guarantee 1 mm of accuracy.

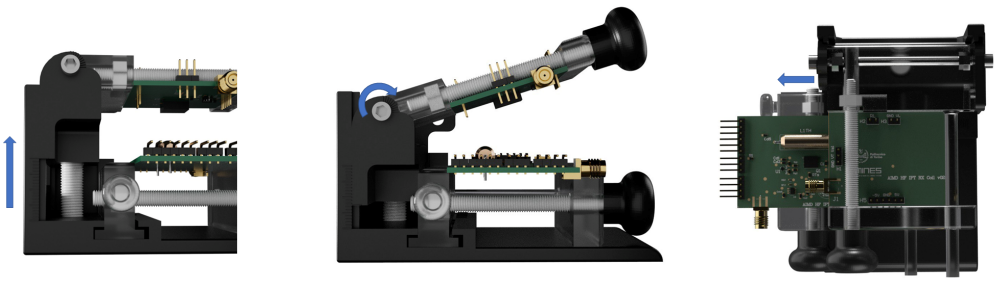

(a) Distance **(b)** Angle **(c)** Misalignment

Figure 6.3: Testbench Degrees of Freedom

6.2 Measures of Class-E PA points of interest

The Class-E PA points of interest to be studied have been previously analyzed [Ch. 4] and comprise:

- Transistor voltage and current behavior compared with the input square wave
- Transmitter coil voltage and current behavior
- Receiver coil voltage and current behavior
- Input current

The current measures were obtained through an elaboration of the current sensing output voltages: the waveforms measured have been imported on Python and divided by the product of the amplifier gain and the shunt resistor value.
Figure 6.4 shows the GS0650041L and the 2N7000 voltage and current behavior, compared with the input square wave. The results are close to the ideal condition of Gate and Transistor voltages, being accurately alternated. The transistor voltage fluctuations are comparable to ringing noise due to parasitic capacitance.
The current measures have a high-frequency component superimposed on the 13.56MHz waveform, which could be noise introduced by the current sensing circuits or the actual transistor current behavior. The average power dissipated in the transistor was respectively 155 mW for the GS0650041L Class-E PA and 210 mW for the 2N7000 Class-E PA.
The Class-E input current, measured from the DC power supply, was equal to

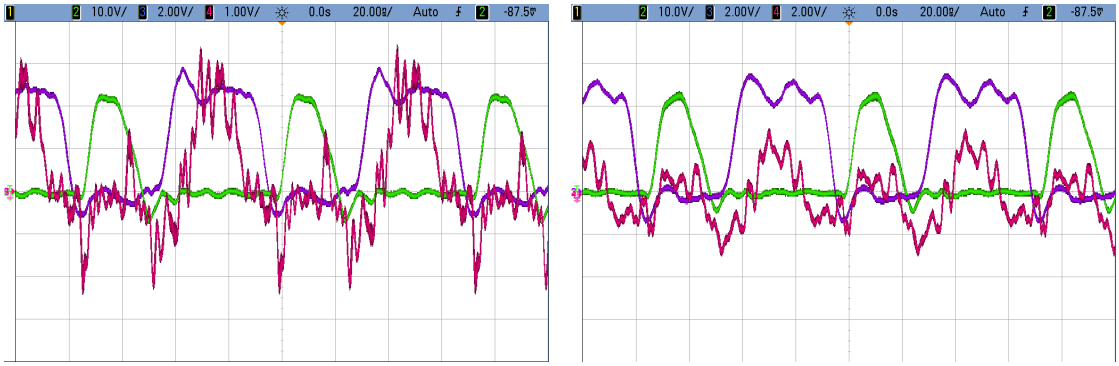

(a) V_G, VC1, and I_D of GS0650041L **(b)** V_G, VC1, and I_D of 2N7000

Figure 6.4: Class-E PA transistor waveforms behavior

152 mA and 280 mA, respectively for the 2N7000 and the GS0650041L configuration. When the oscilloscope probe was attached to the VL2 test point, a decrease correspondingly of 137 mA and 150 mA in the input current was observed. The measures are consequently affected by errors; the transmitted power and the relative PA efficiency are useless to calculated.
LTspice has been used to better understand the origin of the problem, simulating the equipment parasitics: a 14 pF capacitance and a resistance of 1 $M\Omega$ were put in parallel to the coil L2. The current across the power choke inductor decreases also in the simulation: the probe parasitics, being in parallel to the coil, modify the behavior of the circuit [Fig. 6.5].
Potential solutions have been investigated; in particular, the circuit of Figure 6.6 has been implemented on LTspice.

A voltage divider was put in parallel to the transmitter, followed by a voltage follower; measuring the IC output voltage, the parasitic capacitance of the probe is

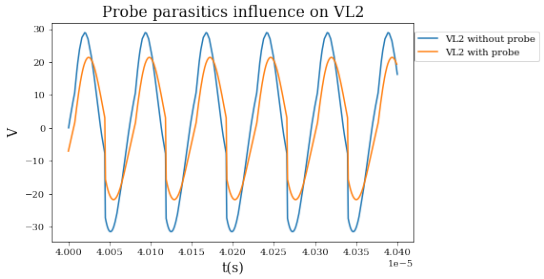

(a) VL2 behavior with and without the probe parasitics

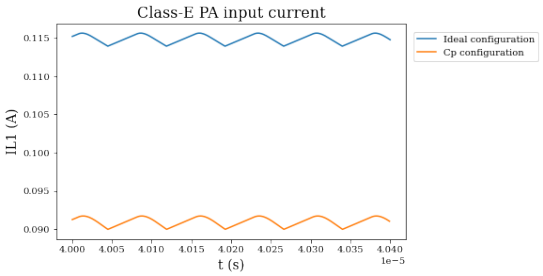

(b) IL1 behavior with and without the probe parasitics

Figure 6.5: Analysis of the influence of the probe parasitics on the voltage across the coil and the input current behavior

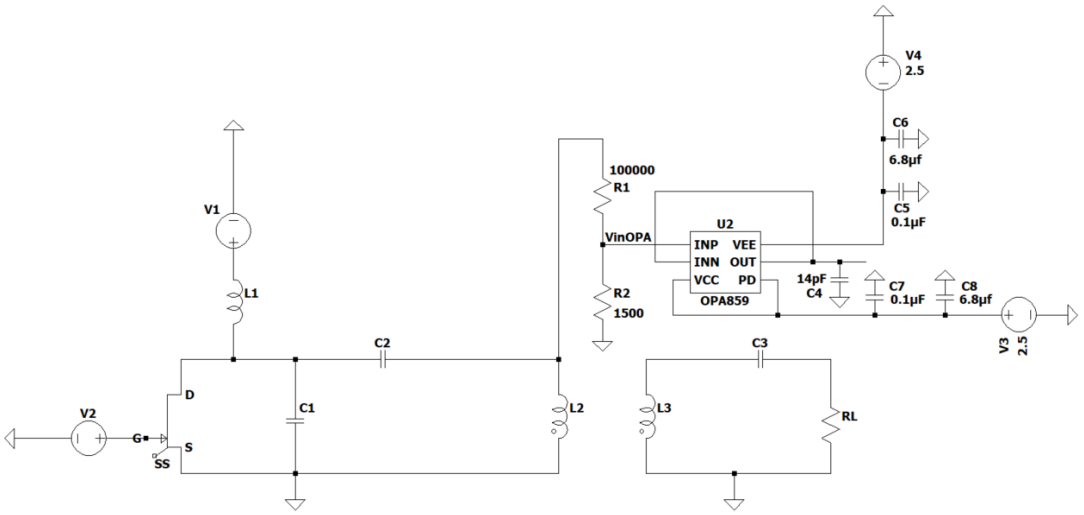

Figure 6.6: Schematic of the Class-E PA with the voltage sensing circuit

in parallel to the high impedance output of the Opamp and should not affect the circuit behavior.
The OPA859, a 900 MHz GBW Opamp, was considered in this simulation. It was configured to be used as a voltage follower, powered between ±2.5 V. The voltage divider ratio has been investigated considering an expected maximum amplitude of $120\,V_{\mathrm{PP}}$ and minimum of $40\,V_{\mathrm{PP}}$:

$$\frac{R2}{R1}_{MIN} = \frac{120V_{PP}}{5V_{PP}} = 24 \tag{6.1}$$

The resistance values that satisfy this constraint have been investigated.
The solution that minimally influences the circuit behavior has R1 equal to 100 kΩ

and R2 equal to 1.5 kΩ; the OPA859 output voltage obtained is equal to the voltage expected from the theoretic equation of the voltage divider:

$$V_{OUT} = VL2\frac{R2}{R1 + R2} \tag{6.2}$$

The voltage divider ratio is 66; consequently, the amplitude of the waveforms is expected to fall in the range between 600 mV_{PP} and 1.8 V_{PP}, readable by the MSO7104A oscilloscope. The dynamic of the amplifier has not been completely used because of the results of Figure 6.7. By increasing R2 above 1.5 kΩ, the input impedance of the OPA859 changes the behavior of the circuit, reducing the output voltages expected and generating a phase shift. Once R2 was sized, the highest value of R1 that satisfies the minimum input voltage expected to be read, has been set.

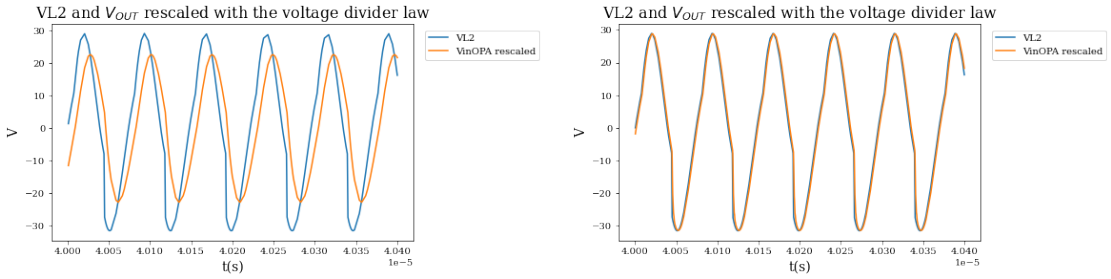

(a) R1=1 MΩ R2=15 kΩ **(b)** R1=100 kΩ R2=1.5 kΩ

Figure 6.7: Comparison of the output voltage with two different voltage divider configurations

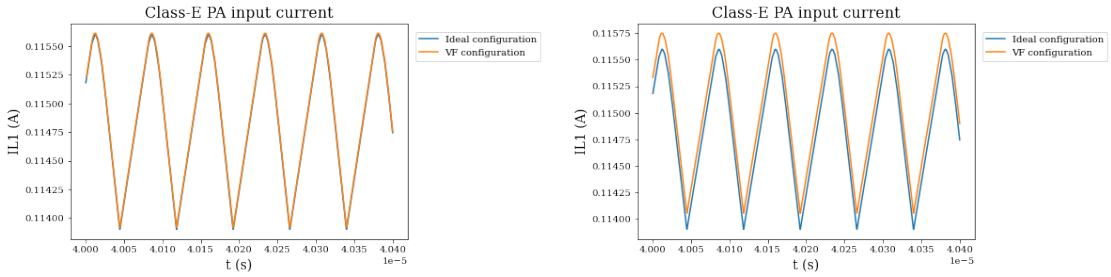

(a) R1=1 MΩ R2=15 kΩ **(b)** R1=100 kΩ R2=1.5 kΩ

Figure 6.8: Comparison of the Class-E input current with two different voltage divider configurations

With R1 equal to 100 kΩ, the input current decreased is negligible; this is the best trade-off that has been found to maintain unchanged the input current IL1 and to guarantee an output voltage that respects Equation 6.2.
Regarding the receiver, the probe parasitics do not influence the behavior of the current and voltage waveforms; consequently, the total efficiency has been evaluated and analyzed in the following section.

6.3 Behavior of total efficiency with changes in distance, misalignment, angle, and input voltage

Total efficiency is not the efficiency of greatest interest in a WPT Class-E PA design. The receiver and the inductive link worsen the PA efficiency, especially if they are not optimized as in this project. The difficulties previously explained in measuring the coil voltage do not allow the PA efficiency to be measured, by estimating the total efficiency, a lower limit can be established.
Figures 6.9, 6.10 show the total efficiency and the received power behavior with

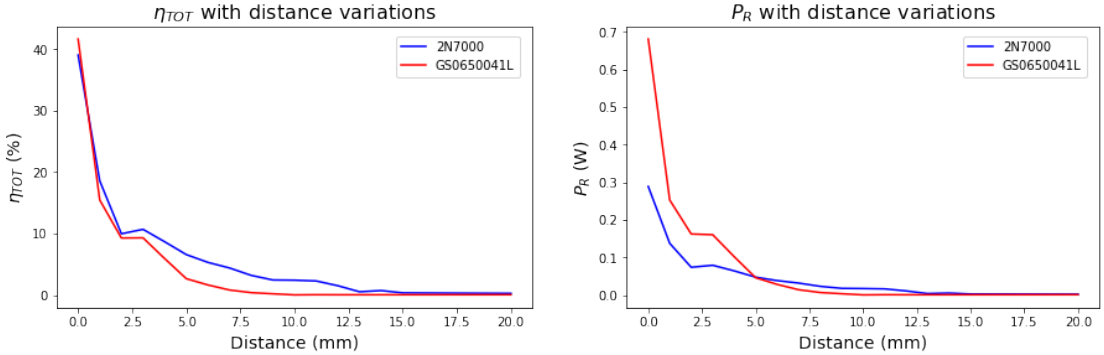

(a) η_{TOT} comparison for the two configurations produced

(b) P_R comparison for the two configurations produced

Figure 6.9: Comparison of η_{TOT} and P_R varying the receiver-transmitter distance

changes in distance and misalignment. It could be observed that performance decreased rapidly in both figures, but less rapidly in the misalignment variations.. With the Tx and Rx coil perfectly aligned and attached, the efficiency is 39 % and 41 % for the 2N7000 and the GS0650041L Class-E PA. Their value rapidly decreases below 10% after 3mm of distance, meanwhile, they are more robust to lateral misalignment variation.
The GS0650041L configuration draws more current than the 2N7000 Class-E but

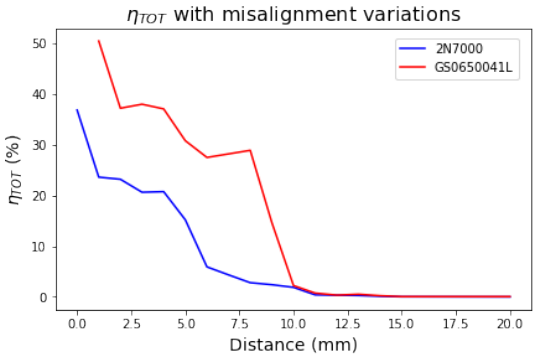

(a) η_{TOT} comparison for the two configurations produced

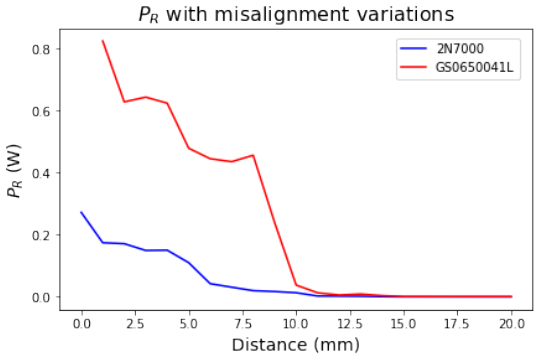

(b) P_R comparison for the two configurations produced

Figure 6.10: Comparison of η_{TOT} and P_R varying the receiver-transmitter lateral misalignment at a distance of 5mm

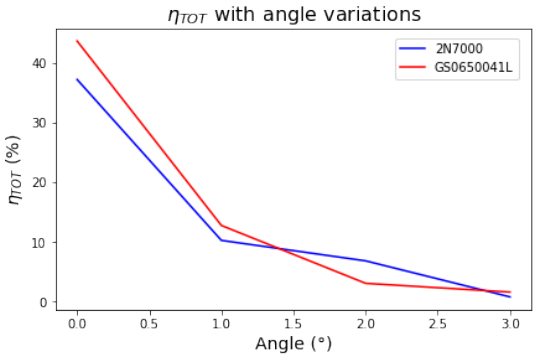

(a) η_{TOT} comparison for the two configurations produced

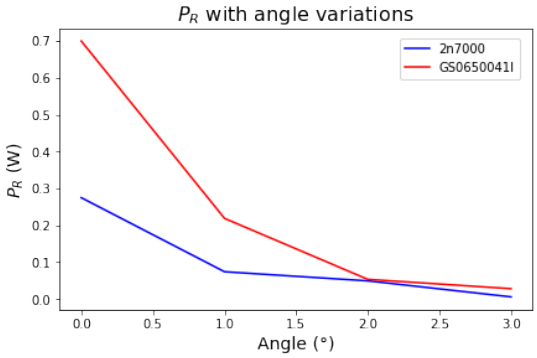

(b) P_R comparison for the two configurations produced

Figure 6.11: Comparison of η_{TOT} and P_R varying the receiver-transmitter angle

also shows more received power for short distances, 392 mW more at 1 mm. The received power by the two configurations becomes 42 mW at 5 mm; at 10 mm the 2N7000 Class-E receives 16 mW while the GS0650041L receives 5 mW. At these distances, the voltages measured become low and comparable to noise, with poor accuracy; at 10 mm, the amplitude of the voltage across the shunt resistor is 40 mV_{PP} in the GS0650041L configuration.

Figure 6.11 shows performance behavior as the angle changes; in this case, both efficiency and power rapidly decrease, also because of the testbench setup: the two coils are welded to the center of the PCB at a distance from the rotation center of 45 mm; as the angle increases, the distance between the coils increases rapidly.

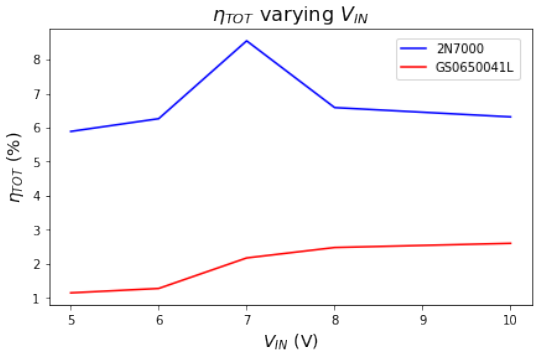

(a) η_{TOT} comparison for the two configurations produced

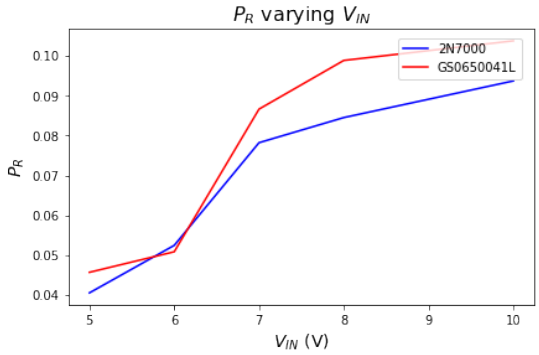

(b) P_R comparison for the two configurations produced

Figure 6.12: Comparison of η_{TOT} and P_R varying the input voltage at a distance of 5mm

Figure 6.12 shows the increase in received power at a distance of 5 mm, by increasing the input voltage from 5 V to 10 V. The received power at 5 mm from the two configurations was similar, in the range between 40 mW and 50 mW. Raising the input voltage to 10V, the received power grew to 100 mW and 93 mW for the GS0650041L and the 2N7000 configurations, respectively. This behavior shows the possible implications of a future introduction of ASK modulation previously introduced [Sec. 2.6].

6.4 Coil temperature behavior

The voltage generated by the NTC thermistor was measured and converted to the relative NTC resistance on the Arduino UNO through the following equation:

$$R_{NTC} = \frac{R1}{\frac{E}{V_U} - 1} \tag{6.3}$$

Then the relative temperature was evaluated through the coming two-parameter model:

$$R_T = R0e^{B(\frac{1}{T} - \frac{1}{T0})} \tag{6.4}$$

B is the characteristic temperature parameter provided by the manufacturer. The 103-JT-025 has B equal to 3.345 K. R0 is the resistance at the temperature T0; in this case, R0 is 10 kΩ, and T0 is 298.15 K. T is the actual temperature; it is evaluated in Celsius degrees through the following equation implemented on the microcontroller board.

$$T = \frac{B}{\log(\frac{R_{NTC}}{R0}) + \frac{B}{T0}} - 273.15 \tag{6.5}$$

The sensitivity of the measures has been evaluated, the range of temperature expected to be read has been set between 10°C and 100°C.
The relative output voltage has been calculated for each i-temperature in the range, with steps of 0.1°C :

$$V_O(i) = 5\frac{R_T}{R1(i) + R_T} \tag{6.6}$$

Afterward, the maximum voltage was checked to be lower than the reference voltage of the ADC (5 V), and the sensitivity has been calculated.

$$S = \frac{V_{O(MAX)} - V_{O(MIN)}}{T_F - T_I} \tag{6.7}$$

A sensitivity of 0.0310°C was found. The temperature T obtained is then displayed on the serial monitor, and the data have been saved on a .txt file through a python script.

The behavior of the temperature in the first 20 minutes of activity of the circuit is shown in Figure 6.13.

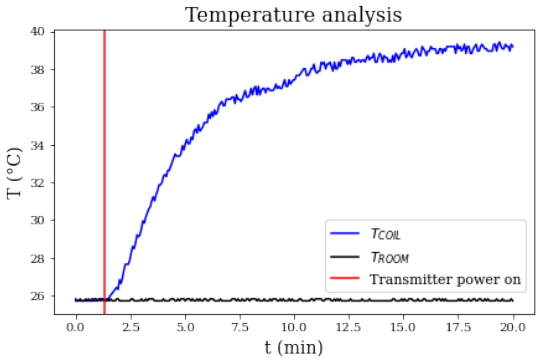

(a) Coil and room temperature measured for 18 minutes after the system power on

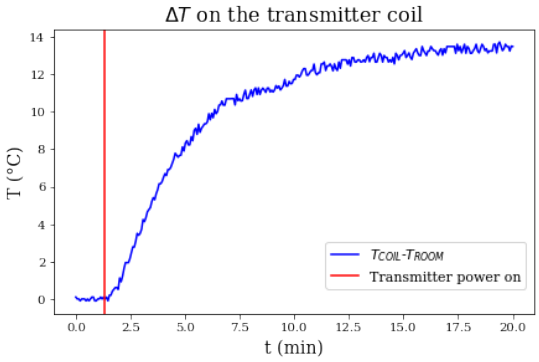

(b) Delta Coil and room temperature measured for 18 minutes after the system power on

Figure 6.13: Coil temperature measurement

It can be observed that from the initial room temperature of 25.75°C, the temperature increases to 39°C after 15 minutes; then, the temperature stays stable. The surface temperature of an implanted device is only allowed to rise 2 °C over the body's normal temperature of 37 °C under the limits imposed by European Standard EN45502-1 [36]. Since the transmitter is external to the body, the temperature reaches the higher limit; however, the transmitter is not implanted and does not have these strict requirements.

Chapter 7

Conclusion

Class-E PA used for Wireless power transfer (WPT) transmitter technologies in AIMDs devices has been discussed. According to the State of Art in Class-E PA design, two different configurations of Class-E PA operating at 13.56 MHz, differing in the transistor technology used (the 2N7000 configuration implements MOSFET technology while the GS0650041L implements GaN technology) have been designed and compared. A simple receiver has been designed to verify the functioning of the system. The system has been first designed and evaluated on LTspice, and afterward, it has been developed on PCB.
The python optimization algorithm, implemented for Class-E PA design, allows the transistor voltage constraint to be achieved. The simulation results show a Power Amplifier efficiency at a distance of 6mm equal to 89.4% and 95.7%, and overall efficiency of 88.6% and 94.8%, for the 2N7000 and the GS0650041L configuration respectively.
The tests on the PCB confirm the achievement of the transistor voltage constraint for both configurations, with results comparable to those of the simulations; the overall efficiency of the system has been studied, including changing distance, lateral misalignment, and angle. The results show a different behavior of the simulation outputs, which indicate the poor reliability of LTspice results when changing the distance through the auto-inductive coefficient. The maximum efficiency is reached at a distance of 1mm, and it is equal to 41.6% and 39%, respectively for the GS0640041L and the 2N7000 Class-E PA.
The overall efficiency rapidly decreases with changes in the spatial parameters due to poor coupling and receiver efficiency. The Power Amplifier efficiency could not be calculated due to the influence of equipment parasitics on voltage measurements; RF measures are highly sensitive to parasitics, and the results obtained show that the equipment could easily introduce errors in the measures; further examinations are necessary to properly conduct RF measurements.

The transmitter coil shows a temperature rise of 14 °C above room temperature after 15 minutes of operation, it reaches a maximum temperature of 39.6 °C.
To better exploit the capability of the system developed, further investigations are needed, listed in order of relevance:

- Development of accurate circuit measurement
  - development and research of voltage measurement circuit, so as not to influence the measurements with the equipment parasitics; a possible circuit solution has been proposed in Section 6.2, where the problem has been analyzed on LTspice, but further investigations are recommended to increase the measurement accuracy.
  - study of different possibilities to the current sensing circuit developed, especially on the receiver circuit where the voltage measured should be higher for accuracy reasons.
- Inductive link and receiver optimization
  - Investigate other coil solutions and eventually design a specific coil to the application that reaches the constraints given by the size and the carrier frequency.
  - Develop a receiver optimized to increase the link and receiver efficiency as much as possible.
- Modulator
  - Development of a modulator to ensure a power threshold at different distances; different solutions have been shown in Section 2.6. The results of received power varying the input voltage are a proof of concept of the ASK modulator, but it is recommended to study which solution to adopt after the measurements have been properly defined and the optimized receiver has been developed.

The present work led to the realization of the first prototype of a WPT Class-E PA transmitter; both the 2N7000 and the GS0650041L configurations satisfy the transistor voltage behavior constraint, usually evaluated in the literature to ensure the correct functioning of the Class-E PA [19, 21]. The optimization algorithm developed in Python allows, in future perspectives, an easier, automatic design of Class-E Power Amplifiers.
The study and implementation of the suggested investigations are recommended to better understand the capabilities of the system and to properly compare the performance between WPT systems operating in the kHz and MHz ranges.

Bibliography

[1] FDA. *Winning in implantable medical devices market: Pharma's next frontier*. URL: https://www.fda.gov/medical-devices/investigational-device-exemption-ide/ide-definitions-and-acronyms#:~:text=Implant%5C%20is%5C%20a%5C%20device%5C%20that,Institutional%5C%20Review%5C%20Board%5C%20(IRB). (accessed: 26.07.2022) (cit. on p. 1).

[2] Achraf Ben Amar, Ammar B. Kouki, and Hung Cao. "Power Approaches for Implantable Medical Devices". In: *Sensors* 15.11 (2015), pp. 28889–28914. ISSN: 1424-8220. DOI: 10.3390/s151128889. URL: https://www.mdpi.com/1424-8220/15/11/28889 (cit. on p. 1).

[3] E. Meng and R. Sheybani. "Insight: implantable medical devices". In: *Lab Chip* 14 (17 2014), pp. 3233–3240. DOI: 10.1039/C4LC00127C. URL: http://dx.doi.org/10.1039/C4LC00127C (cit. on p. 1).

[4] Massimo Zecchin et al. "Seventeen-year trend (2001–2017) in pacemaker and implantable cardioverter-defibrillator utilization based on hospital discharge database data: An analysis by age groups". In: *European Journal of Internal Medicine* 84 (2021), pp. 38–45. ISSN: 0953-6205. DOI: https://doi.org/10.1016/j.ejim.2020.09.003. URL: https://www.sciencedirect.com/science/article/pii/S0953620520303484 (cit. on p. 1).

[5] Sadeque Reza Khan, Sumanth Kumar Pavuluri, Gerard Cummins, and Desmulliez. "Wireless Power Transfer Techniques for Implantable Medical Devices: A Review". en. In: *Sensors (Basel)* 20.12 (June 2020) (cit. on p. 2).

[6] SGA Knowledge Team. *Winning in implantable medical devices market: Pharma's next frontier*. URL: https://us.sganalytics.com/blog/winning-in-implantable-medical-devices-market-pharmas-next-frontier/. (accessed: 26.07.2022) (cit. on p. 2).

[7] Ian Williams, Emma Brunton, Adrien Rapeaux, Yan Liu, Song Luan, Kianoush Nazarpour, and Timothy G. Constandinou. "SenseBack - An Implantable System for Bidirectional Neural Interfacing". In: *IEEE Transactions on Biomedical Circuits and Systems* 14.5 (2020), pp. 1079–1087. DOI: 10.1109/TBCAS.2020.3022839 (cit. on p. 3).

[8] Nicola Di Trani et al. “Remotely controlled nanofluidic implantable platform for tunable drug delivery”. In: *Lab on a Chip* 19 (June 2019). DOI: 10.1039/C9LC00394K (cit. on p. 3).

[9] Kush Agarwal, Rangarajan Jegadeesan, Yong Xin Guo, and Nitish V. Thakor. “Wireless Power Transfer Strategies for Implantable Bioelectronics”. English (US). In: *IEEE Reviews in Biomedical Engineering* 10 (2017), pp. 136–161. ISSN: 1937-3333. DOI: 10.1109/RBME.2017.2683520 (cit. on p. 5).

[10] Maysam Ghovanloo Pablo Pérez-Nicoli Fernando Silveira. “Inductive Links for Wireless Power Transfer”. In: (). DOI: https://doi.org/10.1007/978-3-030-65477-1 (cit. on pp. 6, 7, 23, 64).

[11] Zhihua Wang Tianjia Sun Xiang Xie. “Wireless Power Transfer for Medical Microsystems”. In: (). DOI: https://doi.org/10.1007/978-1-4614-7702-0 (cit. on p. 6).

[12] Yujing Zhou, Chunhua Liu, and Yongcan Huang. “Wireless Power Transfer for Implanted Medical Application: A Review”. In: *Energies* 13.11 (2020). ISSN: 1996-1073. DOI: 10.3390/en13112837. URL: https://www.mdpi.com/1996-1073/13/11/2837 (cit. on p. 6).

[13] Daniel K. Freeman and Steven J. Byrnes. “Optimal Frequency for Wireless Power Transmission Into the Body: Efficiency Versus Received Power”. In: *IEEE Transactions on Antennas and Propagation* 67.6 (2019), pp. 4073–4083. DOI: 10.1109/TAP.2019.2905672 (cit. on p. 8).

[14] Saad Mutashar, M. A. Hannan, Salina Samad, and Aini Hussain. “Development of Bio-Implanted Micro-System with Self Recovery ASK Demodulator for Transcutaneous Applications”. In: *Journal of Mechanics in Medicine and Biology* 14 (Mar. 2014), 1450062 (23 pages) (cit. on pp. 8, 13, 23).

[15] Tommaso Campi, Silvano Cruciani, Federica Palandrani, Valerio De Santis, Akimasa Hirata, and Mauro Feliziani. “Wireless Power Transfer Charging System for AIMDs and Pacemakers”. In: *IEEE Transactions on Microwave Theory and Techniques* 64.2 (2016), pp. 633–642. DOI: 10.1109/TMTT.2015.2511011 (cit. on pp. 8, 9).

[16] electronicsforu. *Harvesting Radio Frequency Energy*. URL: https://www.electronicsforu.com/market-verticals/power-electronics/harvesting-radio-frequency-energy. (accessed: 31.10.2022) (cit. on p. 8).

[17] Matthew Schormans, Virgilio Valente, and Andreas Demosthenous. “Practical Inductive Link Design for Biomedical Wireless Power Transfer: A Tutorial”. In: *IEEE Transactions on Biomedical Circuits and Systems* 12.5 (2018), pp. 1112–1130. DOI: 10.1109/TBCAS.2018.2846020 (cit. on pp. 9, 14, 15, 18, 23).

[18] Saad Mutashar. “Design of Efficient Hybrid E/F Power Amplifier for Biomedical Purposes”. In: 18 (Sept. 2018), pp. 77–85 (cit. on pp. 10, 13).

[19] Pattrawut Srimuang, Nutdechatorn Puangngernmak, and Suramate Chalermwisutkul. “13.56 MHz class E power amplifier with 94.6% efficiency and 31 watts output power for RF heating applications”. In: *2014 11th International Conference on Electrical Engineering/Electronics, Computer, Telecommunications and Information Technology (ECTI-CON)*. 2014, pp. 1–5. DOI: 10.1109/ECTICon.2014.6839809 (cit. on pp. 10, 13, 79).

[20] Nasri Sulaiman, Mokhalad Alghrairi, Roslina Sidek, Mohd Sidek, and Saad Mutashar. “Simple and Efficient Transcutaneous Inductive Micro-System Device Based on ASK Modulation at 6.78 MHz ISM Band”. In: *Tehnicki vjesnik - Technical Gazette* 27 (Oct. 2020), pp. 1478–1485. DOI: 10.17559/TV-20150602203115 (cit. on pp. 10, 13, 23).

[21] Mehdi Lotfi Navaii, Hamed Sadjedi, and Amir Sarrafzadeh. “Efficient ASK Data and Power Transmission by the Class-E With a Switchable Tuned Network”. In: *IEEE Transactions on Circuits and Systems I: Regular Papers* 65.10 (2018), pp. 3255–3266. DOI: 10.1109/TCSI.2018.2808189 (cit. on pp. 10, 13–16, 79).

[22] Mohammad Mahdi Ahmadi and Sima Ghandi. “A Class-E Power Amplifier With Wideband FSK Modulation for Inductive Power and Data Transmission to Medical Implants”. In: *IEEE Sensors Journal* 18.17 (2018), pp. 7242–7252. DOI: 10.1109/JSEN.2018.2851605 (cit. on pp. 10, 16, 24).

[23] Saad Mutashar, M. A. Hannan, Salina Samad, and Aini Hussain. “Efficient data and power transfer for bio-implanted devices based on ask modulation techniques”. In: *Journal of Mechanics in Medicine and Biology* 12 (Aug. 2012). DOI: 10.1142/S0219519412400301 (cit. on pp. 10, 13).

[24] N.O. Sokal and A.D. Sokal. “Class E-A new class of high-efficiency tuned single-ended switching power amplifiers”. In: *IEEE Journal of Solid-State Circuits* 10.3 (1975), pp. 168–176. DOI: 10.1109/JSSC.1975.1050582 (cit. on p. 10).

[25] Tomoharu Nagashima, Xiuqin Wei, Hiroo Sekiya, and Marian K. Kazimierczuk. “Power conversion efficiency of class-E power amplifier outside nominal operation”. In: *2011 IEEE International Symposium of Circuits and Systems (ISCAS)*. 2011, pp. 749–752. DOI: 10.1109/ISCAS.2011.5937674 (cit. on pp. 11, 21).

[26] Andrei Grebennikov. “Switched-mode RF and microwave parallel-circuit Class E power amplifiers”. In: *International Journal of RF and Microwave Computer-Aided Engineering* 14 (Jan. 2004), pp. 21–35. DOI: 10.1002/mmce.10112 (cit. on p. 11).

[27] N.O. Sokal. "Class E-A RF amplifiers". In: *Design Automation, Inc ARRL Technical Advisor* (2001) (cit. on pp. 12, 13, 23, 27, 28).

[28] Analog Devices. *LTspice*. URL: https://www.analog.com/en/design-center/design-tools-and-calculators/ltspice-simulator.html. (accessed: 2.11.2022) (cit. on p. 17).

[29] University of Central Florida. *Power in an AC Circuit*. URL: https://pressbooks.online.ucf.edu/osuniversityphysics2/chapter/power-in-an-ac-circuit/#:~:text=The%5C%20average%5C%20ac%5C%20power%5C%20is,the%5C%20resistance%5C%20by%5C%20the%5C%20impedance. (accessed: 8.11.2022) (cit. on p. 33).

[30] Dr. Steve Arar. *Resistive Current Sensing: Low-Side vs. High-Side Sensing*. URL: https://www.allaboutcircuits.com/technical-articles/resistive-current-sensing-low-side-versus-high-side-sensing/. (accessed: 8.11.2022) (cit. on p. 47).

[31] TI. *Simplifying Current Sensing*. URL: https://www.ti.com/lit/eb/slyy154a/slyy154a.pdf?ts=1667923946831. (accessed: 8.11.2022) (cit. on p. 48).

[32] Dr. Steve Arar. *How to Design High-Frequency PCBs? 11 Clearest Design Rules in 2021*. URL: https://www.allaboutcircuits.com/technical-articles/understanding-the-amplifier-offset-voltage-and-output-swing-in-resistive-current-sensing/#:~:text=The%5C%20offset%5C%20voltage%5C%20is%5C%20defined,swing%5C%20to%5C%20the%5C%20ground%5C%20potential. (accessed: 8.11.2022) (cit. on p. 48).

[33] STMicroelectronics. *AN2653 Application note*. URL: https://www.st.com/resource/en/application_note/an2653-operational-amplifier-stability-compensation-methods-for-capacitive-loading-applied-to-ts507-stmicroelectronics.pdf. (accessed: 10.11.2022) (cit. on p. 52).

[34] PCBONLINE Team. *How to Design High-Frequency PCBs? 11 Clearest Design Rules in 2021*. URL: https://www.pcbonline.com/blog/11-pcb-design-rules-for-high-frequency.html. (accessed: 8.11.2022) (cit. on p. 54).

[35] PCBWay. *High Frequency PCB Layout Techniques*. URL: https://www.pcbway.com/blog/PCB_Design_Layout/High_Frequency_PCB_Layout_Techniques.html. (accessed: 8.11.2022) (cit. on p. 54).

[36] BS EN 45502-1:1998. "Active implantable medical devices. General requirements for safety, marking and information to be provided by the manufacturer, eng". In: (1998) (cit. on p. 77).